PLOS PATHOGENS

RESEARCH ARTICLE

CD56-mediated activation of human natural killer cells is triggered by *Aspergillus fumigatus* galactosaminogalactan

Linda Heilig[1], Fariha Natasha[2], Nora Trinks[2], Vishukumar Aimanianda[3], Sarah Sze Wah Wong[3], Thierry Fontaine[4], Ulrich Terpitz[2], Lea Strobel[1], François Le Mauff[5,6], Donald C. Sheppard[5,6,7,8], Sascha Schäuble[9], Oliver Kurzai[10,11], Kerstin Hünniger[10], Esther Weiss[1], Mario Vargas[12], P. Lynne Howell[12,13], Gianni Panagiotou[9,14,15], Sebastian Wurster[16], Hermann Einsele[1], Juergen Loeffler[1]*

1 Department of Internal Medicine II, University Hospital Wuerzburg, Wuerzburg, Germany, **2** Department of Biotechnology & Biophysics Biocenter, University of Wuerzburg, Wuerzburg, Germany, **3** Department of Mycology, Immunobiology of Aspergillus, Institut Pasteur, Paris, France, **4** Institut Pasteur, Université Paris Cité, INRAE, USC2019, Fungal Biology and Pathogenicity laboratory, Paris, France, **5** Infectious Disease in Global Health Program, McGill University Health Centre, Montreal, Canada, **6** McGill Interdisciplinary Initiative in Infection and Immunity, Montreal, Canada, **7** Department of Microbiology and Immunology, McGill University, Montreal, Canada, **8** Department of Medicine, McGill University, Montreal, Canada, **9** Department of Microbiome Dynamics, Leibniz Institute for Natural Product Research and Infection Biology–Hans Knöll Institute (HKI), Jena, Germany, **10** Institute for Hygiene und Microbiology, University of Wuerzburg, Wuerzburg, Germany, **11** National Reference Center for Invasive Fungal Infections, Leibniz Institute for Natural Product Research and Infection Biology–Hans-Knöll-Institute Jena, Germany, **12** Program in Molecular Medicine, Research Institute, The Hospital for Sick Children, Toronto, Canada, **13** Department of Biochemistry, University of Toronto, Toronto, Canada, **14** Faculty of Biological Sciences, Friedrich Schiller University Jena, Jena, Germany, **15** Faculty of Medicine, Friedrich Schiller University Jena, Jena, Germany, **16** Department of Infectious Diseases, Infection Control and Employee Health, The University of Texas MD Anderson Cancer Center, Houston, Texas, United States of America

* Loeffler_J@ukw.de (JL)

Citation: Heilig L, Natasha F, Trinks N, Aimanianda V, Wong SSW, Fontaine T, et al. (2024) CD56-mediated activation of human natural killer cells is triggered by *Aspergillus fumigatus* galactosaminogalactan. PLoS Pathog 20(6): e1012315. https://doi.org/10.1371/journal.ppat.1012315

Editor: Bruce S. Klein, University of Wisconsin-Madison, UNITED STATES

Received: December 27, 2023

Accepted: June 3, 2024

Published: June 18, 2024

Data Availability Statement: All primary material generated in this study is attached as supporting information (please see S1–S7 Data). All primary sequencing data and processed data described in this manuscript have been deposited in the NCBI Gene Expression Omnibus under the accession numbers GEO: GSE241020; Link: https://www.ncbi.nlm.nih.gov/geo/query/acc.cgi?acc=GSE241020.

Abstract

Invasive aspergillosis causes significant morbidity and mortality in immunocompromised patients. Natural killer (NK) cells are pivotal for antifungal defense. Thus far, CD56 is the only known *pathogen recognition receptor* on NK cells triggering potent antifungal activity against *Aspergillus fumigatus*. However, the underlying cellular mechanisms and the fungal ligand of CD56 have remained unknown. Using purified cell wall components, biochemical treatments, and *ger* mutants with altered cell wall composition, we herein found that CD56 interacts with the *A. fumigatus* cell wall carbohydrate galactosaminogalactan (GAG). This interaction induced NK-cell activation, degranulation, and secretion of immune-enhancing chemokines and cytotoxic effectors. Supernatants from GAG-stimulated NK cells elicited antifungal activity and enhanced antifungal effector responses of polymorphonuclear cells. In conclusion, we identified *A. fumigatus* GAG as a ligand of CD56 on human primary NK cells, stimulating potent antifungal effector responses and activating other immune cells.

Funding: The study was supported by the Deutsche Forschungsgemeinschaft (DFG) within the Collaborative Research Center CRC124 FungiNet "Pathogenic fungi and their human host: Networks of interaction," DFG project number 210879364 (project A2 to UT, HE and JL, C3 to OKu, and INF to GP). VA and TF were supported by the Agence Nationale de la Recherche (ANR) grant ANR-21-CE17-0032-01; FUNPOLYVAC. GP was supported by the BMBF within the funding project PerMiCCion (project ID: 01KD2101A). The funders had no role in study design, data collection and analysis, decision to publish, or preparation of the manuscript.

Competing interests: The authors have declared that no competing interests exist.

Author summary

The opportunistic mold pathogen *Aspergillus (A.) fumigatus* possesses significant health risk, particularly for immunocompromised individuals. This ubiquitous fungus found in soil and decaying organic matter, causes a range of partially life-threatening infections known as aspergillosis. Natural killer (NK) cells, part of the innate immunity, recognize *A. fumigatus* by *pathogen-associated molecular patterns* (PAMPs) via their *pattern recognition receptors* (PRRs), leading to the elimination of infected cells, including direct cytotoxicity and cytokine production. Previously, we identified the NK-cell receptor CD56 as a PRR that recognizes *A. fumigatus* and triggers potent antifungal activity. However, the *A. fumigatus* ligand of CD56 has remained unknown. Here, we used different approaches to identify the *A. fumigatus* ligand of CD56 on NK cells. We found that CD56 directly binds to cell wall galactosaminogalactan. Specifically, deacetylated galactosamine residues of GAG played a role in the interaction with CD56 and triggered strong NK-cell activation, along with potent release of cytotoxic effectors and immune-enhancing chemokines. We also found that GAG-primed NK-cell supernatants activate and enhance effector responses of polymorphonuclear cells. Our study provides new insights on the *A. fumigatus*-NK-cell interplay by identifying GAG as an activating ligand of CD56 on human NK-cells, stimulating potent antifungal effector responses.

Introduction

Invasive pulmonary aspergillosis (IPA), most commonly caused by the opportunistic mold pathogen *Aspergillus fumigatus*, is a devastating infection in immunocompromised patients. Individuals that are highly susceptible to IPA often have neutropenia and/or dysfunctional T-cell responses [1]. This includes patients suffering from hematological malignancies, undergoing allogeneic hematopoietic stem cell transplantation (HSCT) [2,3], with genetic predisposition [4], or suffering from severe respiratory illnesses like Influenza or Covid-19 [5]. IPA poses a major clinical challenge due to limited diagnostic tools, insufficient efficacy of available antifungal therapies, and increasing antifungal drug resistance [3,6,7]. Hence, IPA is associated with high mortality rates [2,8] and poor long-term survival [9]. Thus, understanding host defense and host-pathogen interaction are pivotal for the development of diagnostic biomarkers, targeted anti-virulence agents, and novel immunotherapies.

Several studies have shown that natural killer (NK) cells are an integral part of protective antifungal immunity [10,11]. For instance, HSCT recipients with delayed NK-cell reconstitution or low NK-cell counts are at higher risk of developing IPA, indicating that NK cells are indispensable for fungal clearance [12]. NK cells constitute 5–15% of the blood lymphocyte repertoire and can either secrete regulatory cytokines to recruit and stimulate other immune cells or elicit cytotoxicity against target cells [13,14]. Several mechanisms of NK-cell-mediated cytotoxicity against tumor cells and pathogen-infected cells have been identified. While elimination of target cells through death receptor-mediated apoptosis are critical for NK-cell activity against tumor cells [14–16], this mechanism does not appear to be the main driver of the cells' antifungal activity [17]. Instead, different studies emphasized the importance of lytic granules, containing perforin, granzyme B and granulysin, as mediators of NK-cell cytotoxicity against fungal pathogens [18–20] Besides their direct killing capacity, NK cells are able to release a number of chemokines (CCL3, CCL4, CCL5) and cytokines (IFN-γ) by which they modulate and augment the activity and host response of a number of immune cells such as neutrophils and macrophages [18,21,22].

Innate immune cells, including NK cells, are commonly activated by stimulation of *pattern recognition receptors* (PRR). These receptors detect *pathogen-associated molecular patterns* (PAMPs) of invasive pathogens. Several fungal-reactive PRRs of NK cells have been described. For instance, the natural cytotoxicity receptor (NCR) NKp30 was shown to recognize β-1,3-glucan on the surface of *Candida albicans* and *Cryptococcus neoformans* [23], while the activating human NK-cell receptor NKp46 interacts with the *Candida glabrata* adhesins Epa1, Epa6, and Epa7 [24]. Furthermore, we previously identified the NK-cell receptor CD56 as a PRR recognizing *A*. *fumigatus*. Upon contact with *A*. *fumigatus* hyphae, CD56 relocalizes actin-dependently toward the NK-cell/hyphal interaction site, leading to prominent reduction of CD56-fluorescence intensity. Blocking of CD56 resulted in decreased *A*. *fumigatus*-induced NK-cell activation and chemokine secretion, suggesting a functional relevance of CD56 in hyphal recognition by NK cells [25]. However, while PAMPs for the NK cell receptors NKp46 [24] and NKp30 [23] have been identified, the *A*. *fumigatus* ligand of CD56 has remained unknown.

PAMPs are commonly either microbial structural components (e.g., cell wall polysaccharides) or lipopolysaccharides and are often required for pathogen survival or virulence [23,26]. The cell wall of *A*. *fumigatus* is a complex and dynamic structure, which alters in composition depending on the fungal morphotype and environmental cues [27]. It predominantly comprises polysaccharides and, to a smaller extent, proteins, lipids, and pigments [28]. The main polysaccharides in the cell wall of *A*. *fumigatus* hyphae include chitin, β-1,6-branched β-1,3-glucan, α-1,3-glucan, galactomannan, and galactosaminogalactan [27,28].

Given our prior observation that CD56 solely interacts with *A*. *fumigatus* germ tubes and hyphae but not with conidia, we specifically focused on hyphal PAMPs to identify the *A*. *fumigatus* ligand of CD56. Using a combination of purified cell-wall components, biochemical treatments, and *A*. *fumigatus* mutants, we herein identified galactosaminogalactan (GAG), especially de-*N*-acetylated GAG, as the fungal ligand of CD56. The GAG/CD56 interaction triggered strong NK-cell activation, along with potent release of cytotoxic effectors and immune-enhancing chemokines. Furthermore, supernatants of GAG-pulsed NK cells inhibited fungal growth and enhanced the anti-*Aspergillus* activity of PMNs, suggesting GAG as a potential immunotherapeutic target in IPA.

Results

CD56-mediated recognition of *A*. *fumigatus* depends on intact cell wall polysaccharides

In a first step, we sought to determine whether the binding partner of CD56 on *A*. *fumigatus* hyphae is a cell wall protein or polysaccharide. Therefore, we depleted proteins in the cell wall of *A*. *fumigatus* germ tubes by proteinase K treatment before co-culture with NK cells and flow cytometric quantification of CD56 expression after fungal stimulation. Relocalization of CD56 toward the immunological synapse with *A*. *fumigatus* is accompanied by a remarkable decrease in fluorescence intensity [25]. NK cells confronted with either untreated *A*. *fumigatus* or with proteinase K-treated *A*. *fumigatus* displayed a significant reduction in CD56 fluorescence positivity. (Fig 1A), suggesting that cell-wall-bound proteins are not the ligands of CD56.

Next, we treated *A*. *fumigatus* germ tubes with periodate that oxidizes cell wall polysaccharides having vicinal diols and co-cultured them with NK cells. Compared to NK cells co-cultured with untreated *A*. *fumigatus*, flow cytometry revealed no decrease in NK-cellular CD56-fluorescence intensity when challenged with periodate-treated germ tubes (Fig 1B). This suggests impaired relocalization of CD56 on NK cells co-cultured with periodate-treated

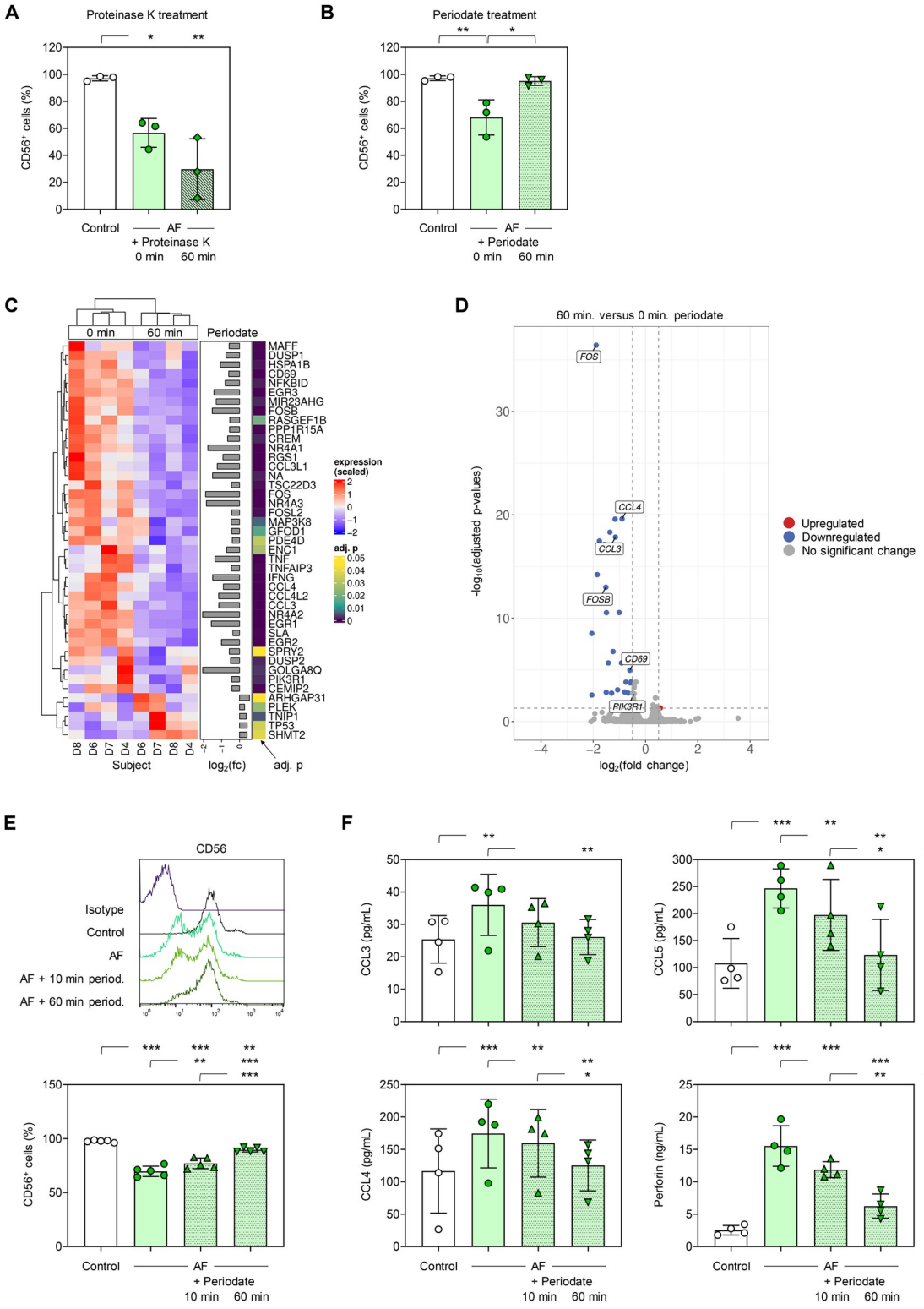

Fig 1. Periodate treatment of *Aspergillus fumigatus* results in loss of binding to NK-cellular CD56 and weakens *Aspergillus fumigatus*-induced NK-cell activation. CD56 expression on naïve NK cells (Control) and NK cells stimulated for 3 h with *A. fumigatus* germ tubes, depending on pre-treatment of the germ tubes with proteinase K (A) or periodate (B). Data for 3 independent donors are shown. (C) Significantly differentially expressed genes after 3-h stimulation of NK cells with *A. fumigatus* germ tubes pre-treated (60 min) with periodate or untreated (0 min). Abbreviations: adj. p = adjusted p-value,

D = donor, fc = fold change. (D) Volcano plot summarizing transcriptional changes in NK cells stimulated with periodate-treated *A*. *fumigatus* germ tubes compared to cells stimulated with untreated germ tubes. Genes with a log2 fold change > 0.5 and an adjusted p-value < 0.05 are highlighted. Selected immune-related genes have been labelled. (E) CD56 expression on naïve NK cells (Control) and NK cells stimulated for 3 h with *A*. *fumigatus* germ tubes, depending on the duration of periodate pre-treatment of the germ tubes. Representative histograms and data for cells from 5 independent donors are shown. (F) Chemokine and perforin release by naïve NK cells (Control) and NK cells stimulated for 3 h with *A*. *fumigatus* germ tubes, depending on the duration of periodate pre-treatment of the germ tubes. (A-B; E-F) Columns and error bars indicate means and standard deviations, respectively. Repeated measures one-way analysis of variance with Tukey's post-hoc test. * $p < 0.05$, ** $p < 0.01$, *** $p < 0.001$.

https://doi.org/10.1371/journal.ppat.1012315.g001

germ tubes. To reinforce these findings, bulk RNA sequencing was performed to identify genes that are differentially regulated in NK cells upon exposure to periodate-treated versus untreated *A*. *fumigatus* germ tubes. NK cells challenged with periodate-treated *A*. *fumigatus* showed 43 significantly differentially expressed genes compared to cells exposed to untreated germ tubes (Fig 1C). Out of these 43 genes, 38 genes (28 with a >0.5 $\log_2$ fold change) had weaker expression in NK cells stimulated with periodate-treated fungus, including genes associated with NK-cell activation (e.g., *CD69*) and chemokine secretion (e.g., *CCL3* and *CCL4*) (Fig 1C and 1D).

Next, we confirmed that declined CD56 interaction of *A*. *fumigatus* after periodate treatment is dependent on the duration of periodate exposure (Fig 1E). Furthermore, periodate treatment time-dependently reduced the ability of *A*. *fumigatus* germ tubes to trigger secretion of macrophage inflammatory protein (MIP)-1α (CCL3), MIP-1β (CCL4), RANTES (CCL5) and perforin from NK cells compared to untreated germ tubes (Fig 1F). Altogether, these results suggest that CD56 on human NK cells interacts with a hyphal cell wall polysaccharide and not a protein.

Binding of CD56 to *A*. *fumigatus* cell wall galactosaminogalactan triggers NK-cell activation

To identify the specific cell wall polysaccharide that binds to CD56, we used an enzyme-linked immunosorbent assay (ELISA), in which different cell-wall polysaccharides extracted from the *A*. *fumigatus* hyphal cell wall were coated on microtiter plates and then incubated with recombinant CD56. Although CD56 interacts only with germ tubes and hyphae of *A*. *fumigatus*, we also tested binding to conidia-specific cell surface components, RodA protein (RodAp) and melanin pigment. Among the tested compounds, CD56 only bound with high affinity and dose-dependently to galactosaminogalactan (GAG), especially its urea-insoluble fraction (Figs 2A and S1A) [29].

Next, we performed a pull-down assay to assess CD56 binding to GAG compared to β-1,3-glucan, the major cell wall polysaccharide of *A*. *fumigatus* (Fig 2B). After interaction with GAG or β-1,3-glucan, CD56 could be extracted from the GAG pellet (lane A) but not from β-1,3-glucan pellet (lane E). Instead, CD56 was found entirely in the supernatant after co-incubation with β-1,3-glucan (lane D). Collectively, these findings suggest a direct and specific interaction between CD56 and GAG.

GAG is a heteropolysaccharide composed of α-1,4-linked monomers of galactose, *N*-acetylgalactosamine (GalNAc), and galactosamine (GalN), synthesized during germination of *A*. *fumigatus* [30,31]. Our CD56 ELISA suggested that CD56 particularly binds to the urea-insoluble GAG fraction (PGG) enriched in GalNAc (Fig 2A). To confirm the specificity of the interaction between PGG and CD56, PGG was coated on ELISA plates and probed with soluble CD56 that has been pre-incubated with acid-hydrolyzed PGG. Indeed, this hydrolysate markedly reduced the binding affinity of recombinant CD56 to PGG (S1B Fig), corroborating that the interaction between PGG and CD56 is specific.

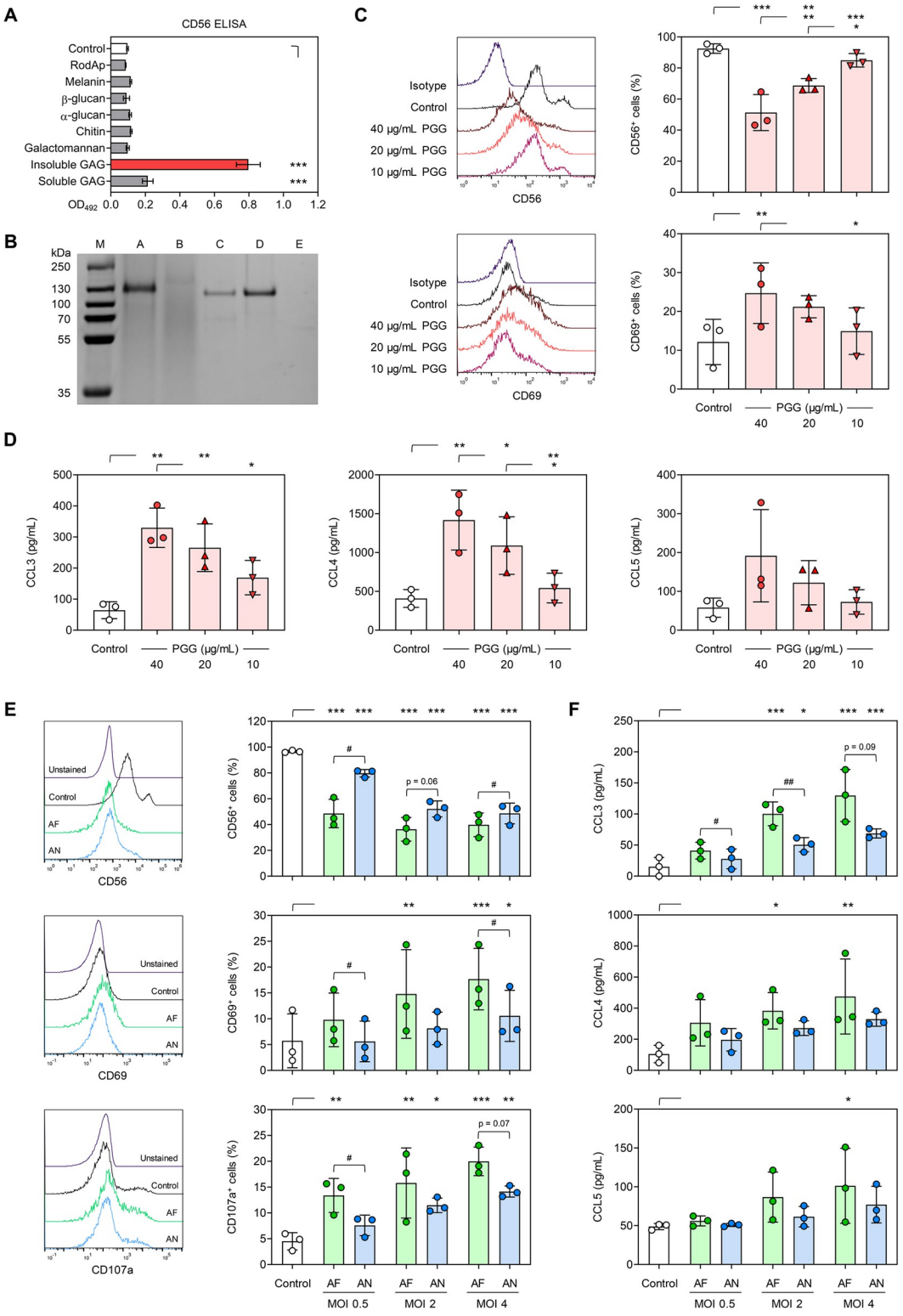

Fig 2. CD56 interacts with *Aspergillus fumigatus* galactosaminogalactan to elicit NK-cell activation. (A) CD56 binding to fungal carbohydrates and proteins, as determined by enzyme-linked immunosorbent assay. GAG = galactosaminogalactan, RodAp = surface rodlet protein/hydrophobin. N = 3 technical replicates. One-way analysis of variance (ANOVA) with Dunnett's post-hoc test versus Control, i.e., no coating. (B) Pull-down assay of CD56 with urea-insoluble galactosaminogalactan (PGG) or β-1,3-glucan. Lane M: Protein marker; Lane A: loading buffer extract of GAG + CD56

pellet; Lane B: supernatant of GAG + CD56; Lane C: CD56 alone; Lane D: supernatant of β-1,3-glucan + CD56; Lane E: loading buffer extract of β-1,3-glucan + CD56 pellet. (C) CD56 and CD69 expression on naïve NK cells (Control) and NK cells stimulated for 24 h with different concentrations of PGG. Representative histograms and data for cells isolated from 3 independent donors are shown. (D) Chemokine release by naïve NK cells (Control) and NK cells stimulated for 24 h with different concentrations of PGG. N = 3 independent donors. (C-D) Repeated measures (RM) one-way ANOVA with Tukey's post-hoc test. (E) CD56, CD69, and CD107a expression on naïve NK cells (Control) and NK cells stimulated for 6 h with *A. fumigatus* (ATCC46645, AF) or *A. nidulans* (ATCC11267, AN) at different multiplicities of infection (MOIs). Representative histograms for one donor at MOI 4 are shown. (F) MOI-dependent stimulation of NK-cellular chemokine secretion after 6-h stimulation with AF or AN. (E-F) N = 3 independent donors. RM one-way ANOVA with Dunnett's post-hoc test versus Control, i.e., unstimulated NK cells (asterisks). In addition, AF and AN stimulation at each MOI was compared using paired t-Test (hash signs). (A-F) Columns and error bars indicate means and standard deviations, respectively. */# $p < 0.05$, **/## $p < 0.01$, *** $p < 0.001$.

https://doi.org/10.1371/journal.ppat.1012315.g002

To test whether PGG also interacts with CD56 on human NK cells, NK cells were stimulated with different concentrations of purified PGG. Using flow cytometry, we detected significant dose-dependent reduction in NK-cellular CD56 fluorescence after stimulation with purified PGG (Fig 2C). Additionally, PGG stimulation led to increased expression of the NK-cell activation marker CD69 (Fig 2C) and induced intracellular IFN-γ production in a dose-dependent manner (S1C Fig). Furthermore, PGG exposure elicited strong secretion of cytotoxic effector molecules (granzyme B and perforin), chemokines (CCL3, CCL4, and CCL5), and IFN-γ from NK cells (Figs 2D and S1D–S1F).

Previous studies found significant differences in cell wall-bound GAG among *Aspergillus* species. Specifically, *A. fumigatus* harbors the highest amount of cell wall-associated GAG, whereas *A. nidulans* produces low quantities of GAG [31]. Therefore, we compared the decrease in CD56 surface expression and NK-cell activation after exposure to *A. fumigatus* and *A. nidulans* at different multiplicities of infection (MOIs). NK cells co-cultured with *A. fumigatus* showed stronger reduction in CD56 fluorescence intensity at all tested MOIs than NK cells confronted with *A. nidulans* (Fig 2E). Likewise, *A. fumigatus* induced stronger surface expression of CD69 and CD107a as well as chemokine secretion than *A. nidulans*, especially at a low MOI (Fig 2E and 2F). These results indicate that the quantity of cell wall-associated GAG plays a role in CD56-mediated NK-cell activation.

CD56 binds to wild-type *A. fumigatus* hyphae but not to mutants lacking GAG

As purified GAG (i.e., PGG) from *A. fumigatus* triggered strong NK-cell activation and cytokine release, we next investigated the potential of the GAG-deficient mutant strains Δ*agd3* [32] and Δ*uge3* [33] to interact with CD56 on NK cells. Therefore, we either co-incubated wildtype (WT) *A. fumigatus* (strain Af293) and the two otherwise isogenic mutants Δ*uge3* and Δ*agd3* (lacking key enzymes for GAG biosynthesis) with soluble CD56 or bovine serum albumin (BSA) protein as control, followed by staining with fluorescent anti-CD56 antibody. Soluble CD56, strongly bound the hyphal surface of *A. fumigatus* WT, but not the hyphal surface of either GAG-deficient mutant (Fig 3A). Upon incubation of *A. fumigatus* WT or the mutants with BSA instead of soluble CD56, we found only dim autofluorescence of the hyphae, ruling out any unspecific binding of the fluorescent antibody to hyphal structure (insert in Fig 3A). In summary, these findings indicate specific binding of CD56 only to the cell wall of *A. fumigatus* WT hyphae that produce functional GAG.

A. fumigatus mutants lacking GAG fail to elicit NK-cell activation

To further strengthen the role of GAG in CD56-mediated hyphal recognition and its potential to induce NK-cell activation, we co-cultured NK cells with *A. fumigatus* WT (Af293) or the

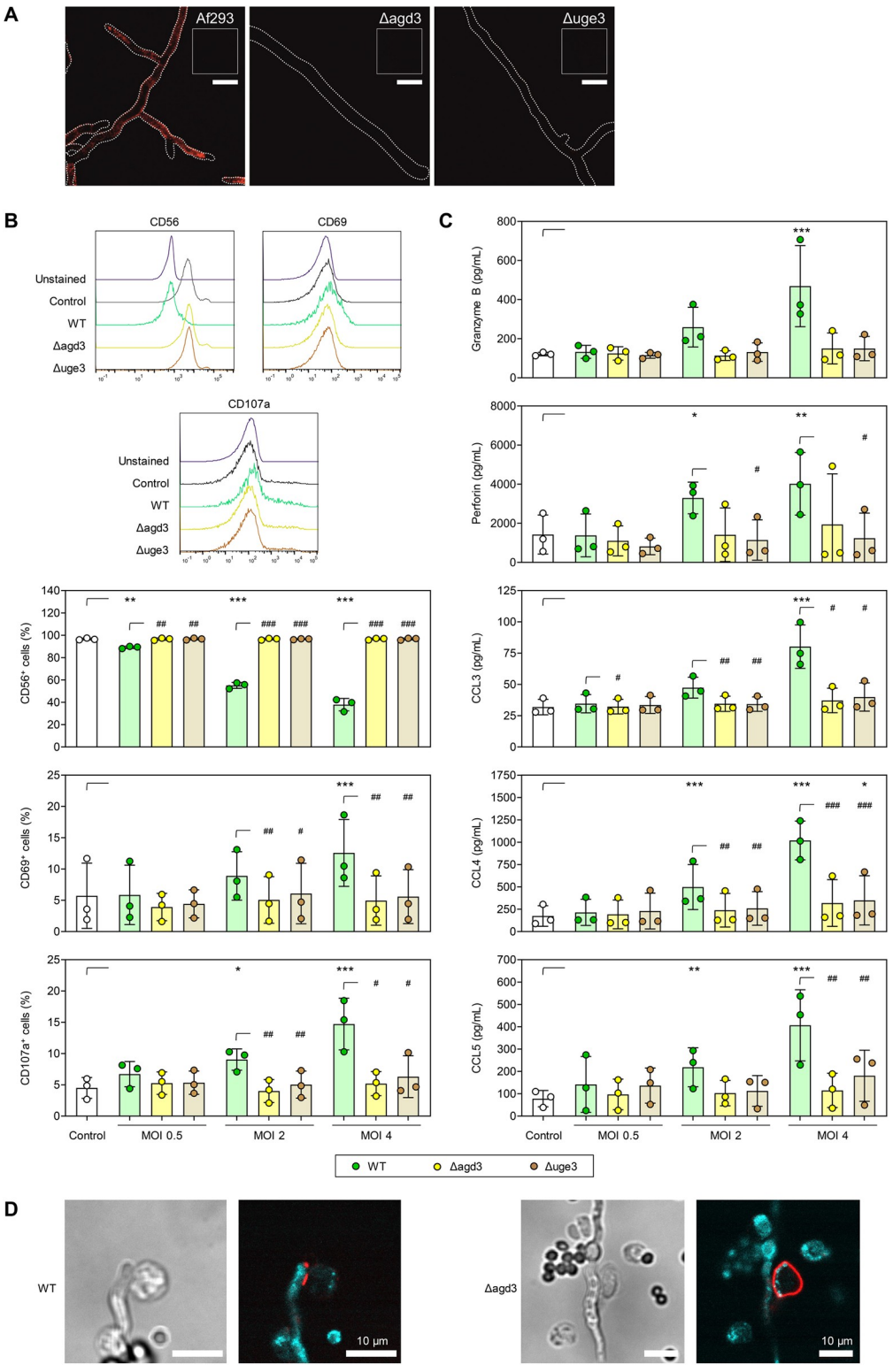

Fig 3. NK cells confronted with galactosaminogalactan-deficient *Aspergillus fumigatus* mutants show impaired activation and weakened chemokine responses and no CD56 accumulation at the *Aspergillus fumigatus*/NK-cell interaction site. (A) Representative fluorescent micrographs (z-projection of 3–4 slices with 1 μm distance, representative dataset from ≥5 independent experiments) of hyphae of wild-type (WT) *A. fumigatus* Af293 and two galactosaminogalactan (GAG)-deficient *A. fumigatus* mutants (Δ*uge3* and Δ*agd3*) co-cultured with soluble CD56,

followed by staining with fluorescent anti-CD56 antibody. The shape of the hyphae is indicated by dotted lines The insets represent a control image (bottom; BSA stained with anti-CD56 antibody) of the respective strain. Scale: 10 μm. (B) CD56, CD69, and CD107a expression on naïve NK cells (Control) and NK cells stimulated for 6 h with WT Af293 or the GAG-deficient *A*. *fumigatus* mutants (Δ*uge3* and Δ*agd3*) at different multiplicities of infection (MOIs). Representative histograms for one donor at MOI 4 are shown. (C) MOI-dependent induction of NK-cellular secretion of granzyme B, perforin, and chemokines after 6-h stimulation with WT Af293, Δ*uge3*, and Δ*agd3*. (B-C) N = 3 independent donors. Repeated measures (RM) one-way analysis of variance (ANOVA) with Dunnett's post-hoc test versus Control, i.e., unstimulated NK cells (asterisks). In addition, results for stimulation with the 3 strains at each MOI was compared using RM one-way ANOVA with Dunnett's post-hoc test versus WT (hash signs). Columns and error bars indicate means and standard deviations, respectively. */# $p < 0.05$, **/## $p < 0.01$, ***/### $p < 0.001$. (D) CLSM micrographs of NK cells co-cultured with WT Af293 and Δ*agd3 A*. *fumigatus* hyphae. CD56 was stained with anti-CD56 Alexa Fluor 647 (red) to assess the CD56 localization. Germ tubes could be detected via their auto-fluorescence (cyan). Scale: 10 μm.

https://doi.org/10.1371/journal.ppat.1012315.g003

GAG-deficient mutants Δ*agd3* and Δ*uge3* at different MOIs. While NK cells confronted with the WT strain showed a marked and MOI-dependent reduction in CD56 fluorescence intensity, no decrease in CD56 expression was observed after co-culture with *A*. *fumigatus* strains lacking Agd3 and Uge3, even at an MOI of 4 (Fig 3B), indicating no accumulation of CD56 at the interaction site of NK cells with the mutant strains. Consistently, NK cells confronted with *A*. *fumigatus* WT hyphae but not with the Δ*agd3* or Δ*uge3* mutant strains showed an MOI-dependent increase in NK-cell activation (CD69) and degranulation (CD107a) (Fig 3B). Consequently, and in contrast to *A*. *fumigatus* WT hyphae, Δ*agd3* and Δ*uge3* mutant strains did not induce secretion of the cytotoxic effector molecules perforin and granzyme B as well as the chemokines CCL3, CCL4, and CCL5 (Fig 3C). This suggests that GAG is involved in *A*. *fumigatus*-induced CD56-mediated NK-cell activation.

GAG is indispensable for CD56 accumulation at the site of *A*. *fumigatus*/ NK-cell interaction

To further corroborate that CD56 on NK cells binds to *A*. *fumigatus* GAG, we incubated NK cells with *A*. *fumigatus* WT hyphae or hyphae of the GAG-deficient strain Δ*agd3* and performed confocal laser scanning microscopy (CLSM) to assess CD56 localization. Consistent with our previous study [25], NK cells co-cultured with the WT strain displayed a strong CD56 signal at the contact site, whereas NK cells exposed to the deacetylase-deficient Δ*agd3* mutant maintained a homogenously distributed CD56 fluorescence signal across the plasma membrane (Fig 3D) [32]. This confirms that CD56 concentrates at the fungal interface in the presence of its ligand GAG.

Deacetylated residues of GAG are crucial for interaction with CD56 and NK-cell activation

Given the absence of CD56 binding to Δ*agd3* mutant hyphae, we further sought to test the importance of deacetylation on the CD56-GAG interplay. We first analyzed CD56 binding to either fully *N*-acetylated GAG (aPGG), fully de-*N*-acetylated GAG (dePGG), and native GAG (PGG), using ELISA. In contrast to native GAG, no binding of aPGG to CD56 was observed, whereas dePGG showed intermediate binding to CD56 (Fig 4A). Incubation of PGG, aPGG, and dePGG with only the secondary antibody or a combination of anti-CD56 and secondary antibody in the absence of recombinant CD56 yielded only a weak background signal, confirming that binding of CD56 to (de)PGG is specific (Fig 4A).

Next, we assessed the capacity of aPGG, dePGG, and native PGG to activate human NK cells. Consistent with the ELISA results, we observed a significant decrease in CD56-fluorescence intensity on NK cells stimulated with native PGG but not with aPGG, while dePGG

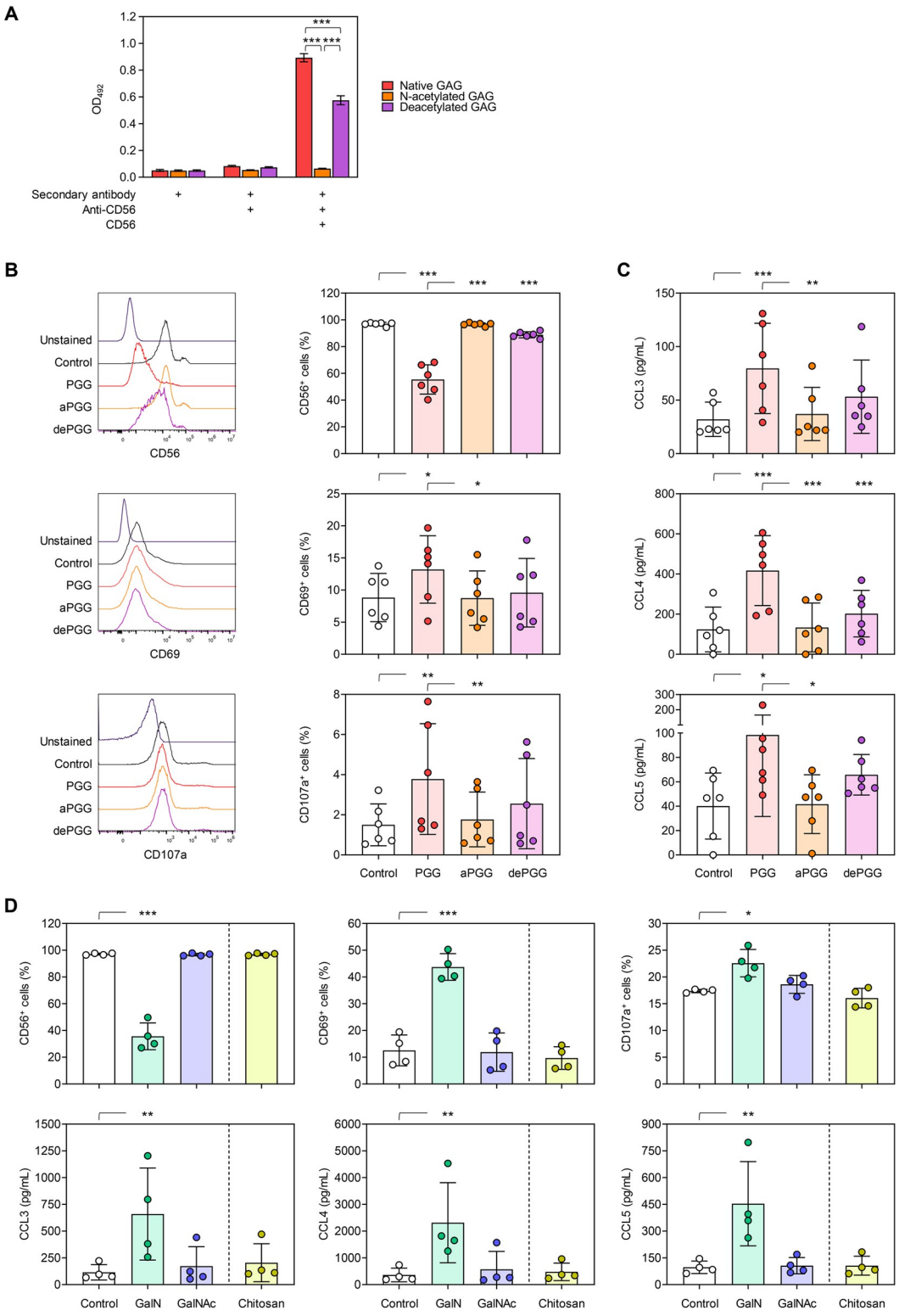

Fig 4. Fully *N*-acetylated PGG and GalNAc oligomers fail to interact with CD56 and elicit no NK-cell activation. (A) CD56 binding to fully acetylated (aPGG), fully deacetylated (dePGG), and native galactosaminogalactan (PGG), was determined by enzyme-linked immunosorbent assay (ELISA). Additional conditions with incomplete ELISA setup were included to preclude unspecific binding of the secondary antibody or anti-CD56 to the carbohydrates. N = 3 technical replicates. One-way analysis of variance (ANOVA) with Tukey's post-hoc test was performed for each assay setup. (B) CD56,

CD69, and CD107a expression on naïve NK cells (Control) and NK cells stimulated for 24 h with PGG, aPGG, or dePGG. Representative histograms for cells isolated from one donor are shown. (C) NK-cellular chemokine secretion after 24-h stimulation with PGG, aPGG, or dePGG. (B-C) N = 6 independent donors. Repeated measures (RM) one-way ANOVA with Tukey's post-hoc test. (D) CD56, CD69, and CD107a expression on naïve NK cells (Control) and NK cells stimulated for 24 h with GalN oligomers, GalNAc oligomers, or chitosan. NK-cellular chemokine secretion after 24-h stimulation with GalN oligomers, GalNAc oligomers, or chitosan. N = 4 independent donors. RM one-way ANOVA with Tukey's post-hoc test. (A-D) * $p < 0.05$, ** $p < 0.01$, *** $p < 0.001$.

https://doi.org/10.1371/journal.ppat.1012315.g004

elicited a modest decrease in CD56-fluorescence positivity. Similarly, stimulation of NK cells with native PGG caused a strong upregulation of CD69 and CD107a expression (Fig 4B), and triggered significant secretion of CCL3, CCL4, and CCL5 (Fig 4C). NK cells incubated with dePGG but not with aPGG showed modest degranulation and secreted slightly higher levels of CCL3, CCL4 and CCL5 compared to unstimulated NK cells (Fig 4C). Collectively, these findings indicate that the degree of deacetylation of GAG plays a role for full CD56-mediated NK-cell activation.

To further elucidate the specificity of the interaction of CD56 with deacetylated galactosamine residues of GAG, we stimulated NK cells with GAG oligomers exclusively consisting of GalN or GalNAc residues. Also, considering the involvement of galactosamine in the interaction with CD56, we investigated the binding affinity of CD56 to chitosan, a polymer composed of de-*N*-acetylated glucosamine and *N*-acetyl-glucosamine units [34,35]. Both, GAG and chitosan are cationic polymers due to their deacetylation [32,34,35]. Interestingly, only NK cells pulsed with GalN oligosaccharides displayed a significant reduction in CD56 fluorescence intensity, along with upregulation of CD69 and CD107a surface expression (Fig 4D). In contrast, GalNAc oligomers were unable to interact with CD56 and induce NK-cell activation. Likewise, chitosan showed neither binding to CD56 nor modulation of CD69 or CD107a (Fig 4D). Consequently, and in contrast to GalN oligomers, GalNAc and chitosan did not stimulate the secretion of chemokines CCL3, CCL4, and CCL5 (Fig 4D). Together, these findings indicate that the presence of galactose residues is not required for the interaction of CD56 with GAG. Moreover, the biochemically similar, positively charged polymer chitosan did not trigger NK-cell activation, further corroborating the specificity of the interaction between CD56 and GAG.

The complete, GalN-rich GAG molecule is required for interaction of CD56 with *A. fumigatus*

To further validate that the complete, GalN-rich GAG molecule is required for CD56-mediated NK-cell activation, we preincubated germ tubes of *A. fumigatus* WT (Af293) or Δ*agd3* with the GAG-specific carbohydrate-active enzymes Sph3 (hydrolase degrading GalNAc homo-oligomers [36]), Ega3 (hydrolase degrading GalN homo-oligomers [37]), and/or Agd3 (deacetylating homo-oligomers [32,38]). As shown above, without enzyme pretreatment, only *A. fumigatus* WT resulted in a prominent reduction in NK-cellular CD56 fluorescence intensity (Fig 5A). Addition of either of the hydrolases or a combination of both to the NK-*A. fumigatus* co-culture alleviated *A. fumigatus* (WT)-induced CD56 relocalization, corroborating CD56 binding to the complete, GalN-rich GAG molecule. Expectedly, pretreatment of Δ*agd3* germ tubes with Agd3, allowing for external complementation of the mutation and GAG deacetylation, significantly decreased NK-cellular CD56 fluorescence intensity to a similar extent as non-pretreated *A. fumigatus* WT. As seen with *A. fumigatus* WT, this effect can be alleviated by addition of hydrolases. As previously observed, all conditions that led to decreased CD56 fluorescence intensity in turn induced enhanced CD69 expression (Fig 5A) and triggered strong production of the cytotoxic effector molecules perforin and granzyme B (Fig 5B).

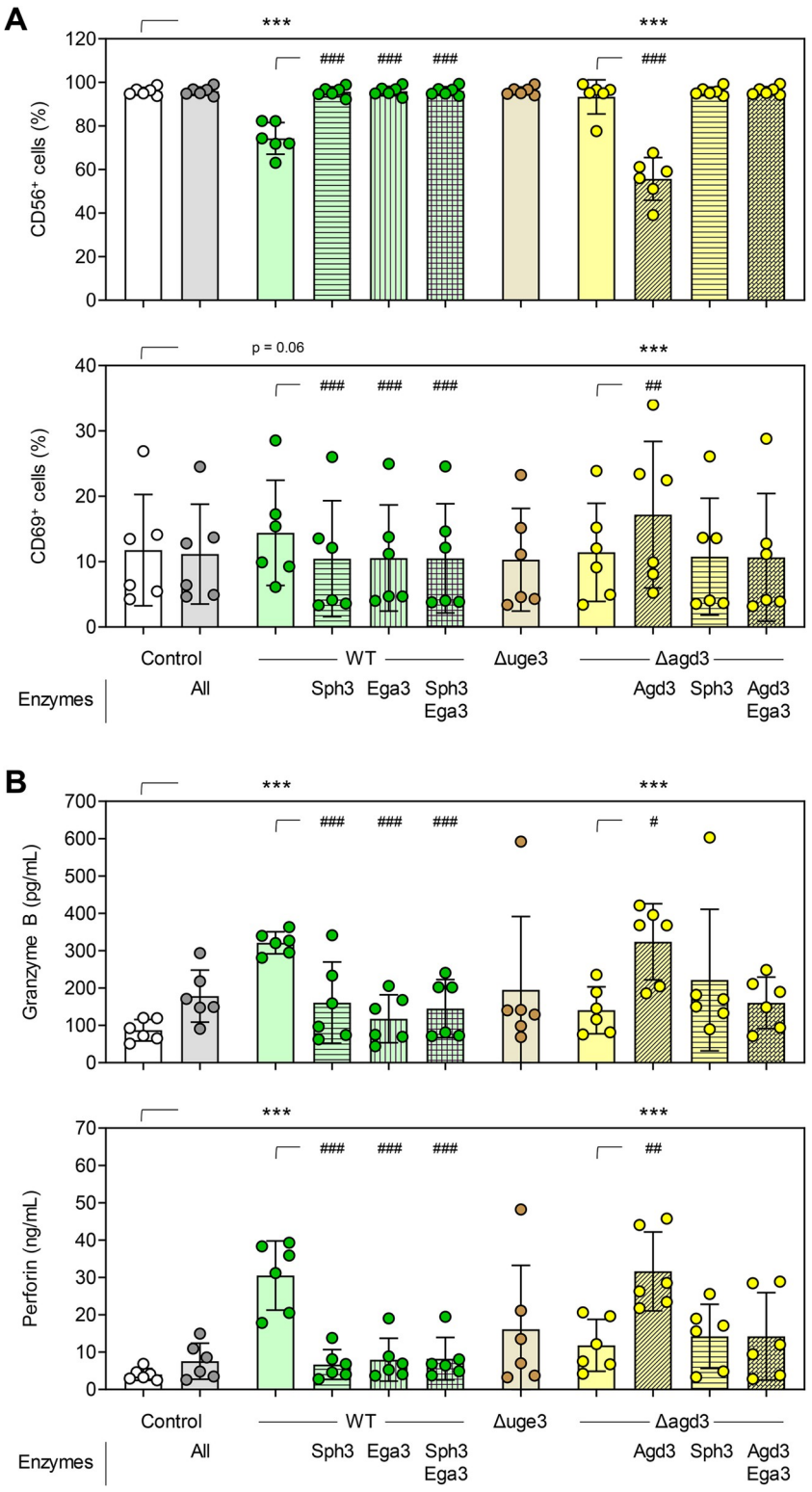

Fig 5. The complete, GalN-rich galactosaminogalactan molecule is required for interaction of CD56 with *Aspergillus fumigatus*. (A) CD56 and CD69 expression of unstimulated NK cells (Control) and *A. fumigatus*-stimulated NK cells (6 h) depending on the fungal strain (wild type [WT] Af293 or isogenic mutants with defective GAG biosynthesis) and its enzymatic pre-treatment. (B) Secretion of granzyme B and perforin by unstimulated NK cells (Control) and *A. fumigatus*-stimulated NK cells depending (6 h) on the fungal strain and its enzymatic pre-

treatment. (A-B) N = 6 independent donors. Repeated measures (RM) one-way analysis of variance (ANOVA) with Dunnett's post-hoc test versus Control, i.e., unstimulated NK cells (asterisks). Additionally, enzymatic pre-treatments of *A. fumigatus* WT and the Δ*agd3* mutant, respectively, were compared using RM one-way ANOVA with Dunnett's post-hoc test versus no enzymatic pre-treatment (hash signs). Columns and error bars indicate means and standard deviations, respectively. */# $p < 0.05$, **/## $p < 0.01$, ***/### $p < 0.001$.

https://doi.org/10.1371/journal.ppat.1012315.g005

Altogether, these data suggest that the intact, GalN-rich GAG molecule is required for CD56-mediated NK-cell activation and release of antifungal effector molecules.

Supernatants of PGG-stimulated NK cells inhibit fungal growth and stimulate polymorphonuclear neutrophils (PMNs)

Next, we sought to assess whether the effector responses induced by CD56/GAG interaction exhibit any anti-*A. fumigatus* activity. Therefore, we used an IncuCyte time-lapse fluorescence microscope and the NeuroTrack image processing algorithm [39] to monitor fungal growth and hyphal branching. Compared to *A. fumigatus* alone, supernatants of NK cells stimulated with PGG significantly inhibited hyphal growth and branching (Fig 6A). In contrast, supernatants of unstimulated NK cells from the same donors did not inhibit fungal growth and morphogenesis (Fig 6A).

In addition to their direct inhibitory effect on fungal growth, we evaluated the capacity of supernatants from PGG-activated NK cells, which contain increased levels of neutrophil-activating chemokines CCL3 and CCL4, to engage PMNs and enhance their anti-*Aspergillus* activity. Expectedly, PMNs partially inhibited fungal growth and hyphal branching of *A. fumigatus* in our IncuCyte NeuroTrack assay. Interestingly, supernatants from PGG-stimulated NK cells significantly enhanced suppression of hyphal growth and morphogenesis by PMNs (Fig 6B), even at a 2.5-fold lower concentration of supernatants from PGG-stimulated NK cells than in our previous experiment (Fig 6A), a concentration that *per se* did not inhibit mycelial proliferation. Additionally, we analyzed *A. fumigatus*-induced ROS production and phagocytosis of *A. fumigatus*-GFP conidia. While supernatants of unstimulated NK cells did not impact neutrophilic ROS response to the germ tubes, PGG-pulsed NK-cell supernatants significantly enhanced *Aspergillus*-induced ROS release of PMNs (Fig 6C). Consistently, supernatants of PGG-pulsed NK cells had a stronger stimulatory effect on phagocytosis of *A. fumigatus*-GFP by PMNs than supernatants of unstimulated NK cells (Fig 6C). Altogether, supernatants of PGG-stimulated NK cells elicited both direct antifungal activity and an indirect immunostimulatory effect through engagement of PMNs

Discussion

While alveolar macrophages and PMNs form the first line of antifungal defense in the lung, NK cells are an integral part of second-line defense against *A. fumigatus*. Several studies showed an involvement of CD56 in NK-cell-mediated cytotoxicity [40–42]. For instance, the deletion of CD56 resulted in failed polarization during immunological synapse formation [43]. We have previously shown that CD56 serves as a PRR for *A. fumigatus* that is required for proper antifungal activity of NK cells [25]. Although the identity of fungal CD56 ligands remained unclear, it was known that only *A. fumigatus* hyphae but not resting conidia are capable to activate NK cells [44]. Herein, we identified GAG as the PAMP of *A. fumigat*us hyphae that interacts with CD56 on NK cells, thereby activating NK cells and inducing potent secretion of chemokines and cytotoxic effector molecules, mirroring previous findings upon *A. fumigatus* stimulation [25,44]. Notably, GAG-deficient mutants or *A. fumigatus* hyphae pretreated with GAG-depleting hydrolases failed to elicit NK-cell activation and secretion of

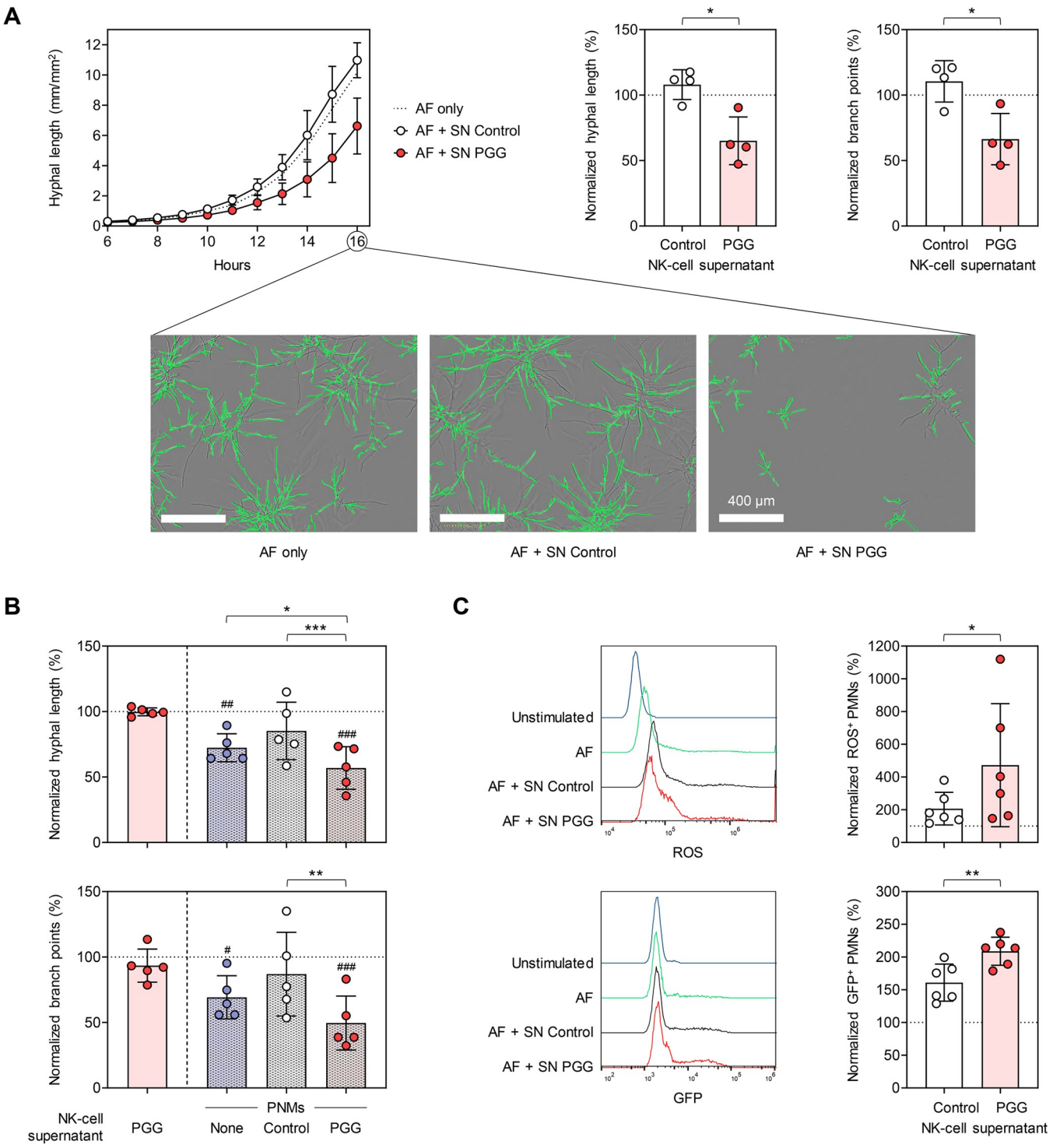

Fig 6. PGG-pulsed NK-cell supernatants confer a direct antifungal effect and engage PMNs into the antifungal immune response. (A) Growth and morphogenesis of ATCC46645-GFP germ tubes in the presence of supernatants from unstimulated NK cells (SN Control) or PGG-stimulated NK cells (SN PGG) was quantified using the IncuCyte NeuroTrack assay and compared to ATCC46645-GFP grown without NK-cell supernatants (AF only). Left panel: Kinetics of hyphal length during transition from germ tubes to hyphae (6–16 h of culture). Center and right panel: Hyphal length and branch point numbers after 16 h of culture, normalized to the "AF only" control (dashed line, 100%). The assay was performed using NK-cell supernatants from n = 4 independent donors. Paired ratio t-test. In addition, images from a representative donor are shown. Green overlays indicate hyphal detection by the NeuroTrack algorithm. (B) Growth and morphogenesis of ATCC46645-GFP germ tubes in the presence of polymorphonuclear neutrophils (PMNs), with or without addition of SN Control or SN PGG, was quantified using the IncuCyte NeuroTrack assay. Hyphal length and branch point numbers after 16 h of culture were normalized to

ATCC46645-GFP grown without PMNs and NK-cell supernatants (AF only, dashed line, 100%). AF grown without PMNs but with SN PGG was used as an additional control. N = 5 pairs of PMNs and NK-cell supernatants. Repeated measures (RM) 1-way analysis of variance and Dunnett's post-hoc test versus "AF only" (hash signs) and "AF + PMNs without supernatant" (asterisks) were used to determine statistical significance of the combined effect of PMNs + supernatants and the impact of the supernatant on PMN-mediated fungal growth inhibition, respectively. (C) Production of reactive oxygen species (ROS) and phagocytosis was assessed upon co-culture of PMNs with *A. fumigatus* in the presence of SN Control or SN PGG for 3 h (ROS production) or 1 h (phagocytosis), respectively. Results were normalized to PMNs confronted with *A. fumigatus* in the absence of NK-cell supernatant. N = 6 pairs of PMNs and NK-cell supernatants. Paired ratio t-test. (A-C) Columns and error bars indicate means and standard deviations, respectively. * $p < 0.05$, ** $p < 0.01$, *** $p < 0.001$.

https://doi.org/10.1371/journal.ppat.1012315.g006

cytotoxic mediators and chemokines, underscoring the functional relevance of the CD56/GAG interaction.

GAG was reported to be located at the surface of the hyphal cell wall and profusely secreted in the extracellular matrix [33] where it plays a critical role in host-pathogen interactions [30]. This polysaccharide is considered a multifunctional virulence factor contributing to biofilm formation [33], host cell adhesion [32,33,45], immune evasion [27], epithelial cell damage [33], and platelet activation[46,47]. Moreover, the level of cell wall GAG production is directly associated with the varying virulence within the *Aspergillus* genus [31].

Purified native GAG bound to CD56 and elicited pronounced NK-cell activation, ruling out that impaired NK-cellular interaction with GAG-deficient hyphae was only due to their impaired adherence [32,33,45]. Moreover, we were able to specifically visualize the interaction of CD56 with hyphal cell wall structures only in GAG-producing *A. fumigatus* but not in GAG-deficient mutants, further corroborating that GAG is essential for hyphal-targeting by NK cells.

GAG composition appears to be critical for recognition by CD56, as *A. fumigatus* Δ*agd3*, which produces GAG that lacks deacetylated GalN residues and therefore cannot stick to the hyphal surface [32], did not show binding to CD56. Given that both *A. fumigatus* Δ*agd3* and purified fully *N*-acetylated PGG showed no interaction with CD56, we conclude that the presence of GalN in GAG is required for the binding of CD56 to GAG. Although both native PGG and fully de-*N*-acetylated PGG displayed binding to CD56, the interaction with fully de-*N*-acetylated PGG was significantly weaker, possibly due to steric hindrance. Purified GalN oligomers but not GalNAc oligomers displayed CD56-binding-affinity and elicited NK-cell activation and chemokine secretion. This finding is consistent with prior reports that the degree of acetylation is an important modulator of the immunostimulatory versus anti-inflammatory properties of GAG [32,48]. Specifically, the role of deacetylated GAG for NLRP3 inflammasome activation through translational inhibition and induction of endoplasmic reticulum stress, in turn promoting protective immunity was highlighted [49]. Deacetylation of acetylated residues renders polymers cationic and introduces biologically unique properties, including adhesion to anionic surfaces such as the hyphal cell wall, plastic, and host cell membranes [32]. However, even though both GAG and chitosan are de-*N*-acetylated polymers with cationic properties [34,35], chitosan did not exhibit immunostimulatory activity on NK cells, corroborating the specificity of the CD56/GAG interaction.

Recently, Picard *et al*. reported distinct effects of CD56 on primary NK-cell function and concluded that CD56 induces NK-cell degranulation, IFN-γ secretion, and morphological changes [50]. Interestingly, that study did not reveal any major impact of CD56 on NK-cellular cytotoxicity. In our setting, we demonstrate that direct CD56/GAG interaction contributes to the release of antifungal effector molecules and cytotoxicity, resulting in the inhibition of hyphal growth, suggesting that GAG-activated NK cells may exert this effect by releasing perforin to reduce hyphal metabolic activity [44]. Other NK-cellular effector functions that were not captured by our experiment with NK-cell supernatants, e.g., death receptor-mediated apoptosis, might also play a role. However, these effects are difficult to study, because the GAG-deficient mutants have altered growth and adhesion characteristics, making unbiased side-by-

side comparisons in co-culture experiments difficult. Our data also showed that chemokine secretion from NK cells upon GAG stimulation leads to enhanced PMN activation and engagement of PMNs into the antifungal immune response. While stimulating NK cells, GAG has been previously shown to contribute to pulmonary immunopathology by promotion of neutrophil apoptosis [29,51], induction of IL1RA secretion [48,52], and activation of the macrophage inflammasome [49]. It is conceivable that NK-cellular cytotoxicity is crucial to overcome GAG-induced immunopathology. This hypothesis could explain the observation that poor NK-cell reconstitution significantly increased IPA risk in allogenic HSCT recipients, even in the absence of other cytopenia [12].

Thus far, detailed CD56 downstream signaling is largely unknown but is likely mediated by different activation kinases such as Syk, PI3K, and Erk [50]. Therefore, functional studies in combination with multimodal CD56 downstream pathway analyses will be an important future direction. Furthermore, our study only focused on the NK cells–GAG interaction without considering other CD56-expressing immune cells, such as T-cell subsets, dendritic cells, and monocytes [53]. CD56 on these cells might also act as a *pathogen recognition receptor* for *A*. *fumigatus* GAG, leading to modulation of their activation status, increased cytokine production, or altered migratory behavior. Further investigation of the crosstalk between *A*. *fumigatus* and CD56-expressing T cells and monocytes could provide insights into the broader immunomodulatory effects of this interaction. Unfortunately, no CD56 knockout mouse model is available, as no immediate CD56 homologue is present in murine NK cells. Therefore, future studies using CD56-deficient human NK cells, e.g., by means of CRISPR/Cas9 to specifically delete CD56, would be needed. Our study is subject to further limitations, including the partial lack of functional data due to the absence of an *in vivo* model for CD56 and the sole use of isolated NK cells without consideration of their complex interplay with other immune cell populations or tissue. Lastly, because this study focused on identifying and characterizing the fungal ligand of CD56, we did not include other fungal PAMPs and human PRRs in our analyses.

In summary, our data shed new light on the distinct *A*. *fumigatus*-NK-cell interaction by providing inaugural evidence that GAG is an activating ligand of CD56 on human NK cells. To our knowledge, in this study, we have identified the first microbial ligand recognized by this receptor. Detailed insights into the specific immunomodulatory cellular signatures and downstream pathways involved in the CD56/GAG interaction could help to develop new alternative antifungal immunotherapies involving NK cells (e.g., chimeric antigen receptor NK cells). Moreover, further insights into the specific immunoregulatory properties and virulence attributes associated with specific biochemical patterns of the GAG molecule could enable the development of new targeted anti-virulence strategies and vaccines against *A*. *fumigatus*.

Methods

Ethics statement

The processing of human peripheral venous blood from healthy adult donors was approved by the Ethics Committee of the University Hospital Würzburg (#302/12). Healthy volunteers donating venous whole blood for isolation of PMNs gave informed written consent.

Peripheral blood mononuclear cell (PBMC) isolation

PBMCs were isolated from leukoreduction chambers obtained from plateletpheresis donations of healthy individuals. PBMCs were isolated by ficoll-histopaque (Sigma-Aldrich, St. Louis, MO, USA, 1.077 g/ml, #10771) density centrifugation. After separation, PBMCs were washed twice with 50 mL of HBSS buffer (Sigma Aldrich, St. Louis, MO, USA, #H6648) supplemented

with 2 mM EDTA (Sigma Aldrich, St. Louis, MO, USA, #E7889) and 1% heat-inactivated fetal calf serum (FCS, Sigma Aldrich, St. Louis, MO, USA, #F7527). Thereafter, PBMCs were counted with a Vi-Cell XR counter (Beckman Coulter, Brea, USA). NK cells were isolated from PBMCs by negative selection using the human NK cell isolation kit (Miltenyi Biotec, Bergisch Gladbach, Germany, Cat#130-092-657). NK cells were cultured in Roswell Park Memorial Institute medium (RPMI, Gibco, Thermo Fisher Scientific, Waltham, MA, USA; #72400021, 1×10^6 cells/mL) supplemented with 10% FCS and 120 μg/ml gentamicin (Gentamicin-ratiopharm, Ulm, Germany) at 37˚C and 5% CO_2. Prior to co-culture experiments, NK cells were stimulated overnight with 1000 U/ml IL-2 (Proleukin S, Novartis, Basel, Schweiz).

Isolation of Polymorphonuclear Granulocytes (PMNs)

PMNs were isolated from 18 mL venous EDTA-anticoagulated blood from healthy donors using PolymorphPrep (ProteoGenix, Schiltigheim, France, #1114683) gradient centrifugation at 590 ×*g* for 30 min. The interphase, containing PMNs, was carefully removed and washed with HBSS for 5 min at 590 ×*g*. To lyse remaining erythrocytes, 5 mL erythrocyte lysis buffer (EL buffer, Qiagen, Hilden, Germany, #79217) was added and PMNs were centrifuged, counted with a hemocytometer, and resuspended in RPMI + 10% FCS. Purity of the PMN suspension was analyzed by flow cytometry (CD3-PerCP$^-$/CD66b-FITC$^+$/CD14-PE^{low} cells > 90%, antibodies from Miltenyi Biotec, Bergisch Gladbach, Germany).

Culture of fungal strains and preparation of germ tubes

A. *fumigatus* strains used in this study included Af293, Δ*agd3* mutant [32], Δ*uge3* mutant [33] (kindly provided by Donald Sheppard McGill University, Montreal, Quebec, Canada), as well as American Type Culture Collection (ATCC) reference strain 46645 and ATCC46645-GFP. In addition, *A*. *nidulans* strain ATCC11267 (Leibniz Institute, DSMZ-German Collection of Microorganisms and Cell Cultures, DSM820) was used. *A*. *fumigatus* and *A*. *nidulans* strains were plated on beer wort agar (Oxoid, Wesel, Germany, PO5055A) and incubated at 35˚C until conidiophores were visible. Conidia suspensions were prepared by rinsing the plates with sterile distilled water and passed through a 20- μm cell strainer (Miltenyi Biotec, Bergisch Gladbach, Germany) to eliminate residual mycelium. To generate germ tubes, 2×10^7 conidia were incubated in RPMI medium (20 mL in 50 mL tubes) at 25˚C while shaking (200 rpm) until small germ tubes were visible. Germ tubes were centrifuged at 5,000 ×*g* for 10 min and resuspended in RPMI medium (4×10^6/mL).

Production of GAG-modifying enzymes

Glycoside hydrolases and deacetylase (gift from the Howell lab, Sick Kids, Toronto), were produced and purified as previously reported (Agd3 [32,38], Sph3 [36,54], Ega3 [37]).

Periodate/ Proteinase K treatment of *A*. *fumigatus* germ tubes

A. *fumigatus* ATCC46645 conidia were seeded in 6-well plates (2×10^5 conidia per well in 2 mL of RPMI medium) and incubated for 18 h at 30˚C. The supernatant was removed, and germ tubes were treated with 2 mL of 10 mM sodium *m*-periodate (Sigma Aldrich, St. Louis, MO, USA, #71859) in RPMI, or 50 μg/mL Proteinase K (Roche, Basel, Switzerland, #41227400) for 60 min in RPMI for 10 min and 60 min, respectively, or were left untreated. Thereafter, wells were washed thrice by replacing two thirds of the supernatant with HBSS buffer supplemented with 2 mM EDTA and 1% FCS. After the last washing step, the washing buffer was completely removed, and 1 mL of pre-warmed RPMI containing 10% FCS was added to the hyphae.

Three million NK cells were added to each well in a final volume of 3 mL per well. *A. fumigatus*/NK-cell co-cultures were incubated for 3 h at 37˚C, 5% CO_2 and subsequently analyzed by flow cytometry. Additionally, the effect of periodate treatment was analyzed by bulk RNA-Seq.

CD56-binding to *A. fumigatus* cell wall polysaccharides and dose-dependent interaction of CD56 with GAG

Polysaccharides of *A. fumigatus* mycelium were extracted and purified as previously reported. Briefly, galactomannan was isolated from mycelium membrane [55]. GAG was purified from culture supernatant [48]. Chitin, β-1,3-glucans and α-1,3-glucans were extracted from cell wall after several chemical treatments [56–58]. Polysaccharides were coated on 96-well microtiter plates (10 μg/well) overnight at room temperature (RT). Wells were blocked with PBS (Gibco, Thermo Fisher Scientific, Waltham, MA, USA, #14200–067) containing 1% BSA (Sigma Aldrich, St. Louis, MO, USA, # A3294) at RT for 1 h, followed by incubation with recombinant CD56 protein (0.1 mg/mL or two-fold serial dilutions between 1 μg- 0.125 μg CliniSciences, Nanterre, France, # CRP2659) in PBS + 1% BSA at RT for 1 h. Wells were washed thrice with PBS + 0.05% Tween 20 (Sigma Aldrich, St. Louis, MO, USA, # P2287) and incubated with anti-CD56 antibody (1:50 in PBS + 1% BSA, CliniSciences, Nanterre, France, #NB-22-63149-20) at RT for 1 h. After three washing steps with PBS + 0.05% Tween 20, wells were incubated with anti-mouse IgG peroxidase-conjugated (1:1000 in PBS + 1% BSA, Sigma Aldrich, St. Louis, MO, USA, #401253) at RT for 1 h, followed by an additional washing step. *O*-phenylenediamine dihydrochloride (Sigma Aldrich, St. Louis, MO, USA, #P5412-50TAB) was added as substrate. Color development was stopped with 4% H_2SO_4 (Sigma Aldrich, St. Louis, MO, USA, #258105-1L-PC) after 20 min. Optical density was measured at 492 nm as a surrogate of CD56 binding. Three independent experiments were performed. For the dose-dependent interaction of CD56 with GAG three technical replicates with two different batches of GAG were used.

Pulldown assay

Soluble CD56 (1 μg) was incubated with 10 μg of insoluble GAG or β-1,3-glucan (extracted from *A. fumigatus*) at 37˚C for 1 h. Thereafter, the contents were centrifuged to collect supernatants; pellets were washed with PBS. Both supernatants and pellets were boiled with SDS-PAGE loading buffer and subjected to SDS-PAGE (on 12% gel).

Inhibition of CD56 binding by GAG oligosaccharides

GAG was subjected to acid hydrolysis with 2 M HCl (Gibco, Thermo Fisher Scientific, Waltham, MA, USA, #H/1200/PC15), 100˚C for 3 h to obtain soluble oligosaccharides of various length (max. 25–28 monosaccharide units), as previously described [29,48]. PGG (10 μg/well) was coated on a 96-well microtiter plate overnight at RT. Recombinant CD56 was pre-incubated with acid-hydrolyzed GAG oligosaccharides at RT for 30 min. The mixture was centrifuged, and the supernatant was added to the PGG-coated microtiter plate and incubated at RT for 1 h. Primary (anti-CD56 antibody 1:50 in PBS + 1% BSA) and secondary (anti-mouse IgG peroxidase-conjugated, 1:1000 in PBS + 1% BSA) antibodies were added at RT for 1 h. *O*-phenylenediamine dihydrochloride was used as substrate to measure absorbance at 492 nm, as described above. Two independent experiments were performed.

NK-cell stimulation with purified GAG, its oligomers, or chitosan

To analyze binding of PGG to CD56 and PGG-induced NK-cell activation, IL-2-pre-stimulated NK cells (2×10^5 cells/well) were incubated with different concentrations (40 μg/mL,

20 μg/mL, 10 μg/mL) of PGG [29] or with 10 μg/mL fully de-*N*-acetylated PGG or *N*-acetylated PGG [48] for 24 h at 37˚C and 5% CO_2. For flow cytometric assessment of intracellular IFN-ɣ production after PGG stimulation, brefeldin A (4 μg/mL, Sigma-Aldrich St. Louis, MO, USA, #B7651), and BD GolgiStop (0.67 μL/mL, BD Biosciences, San Jose, CA, USA, Cat#554724) were added after 6 h of incubation. For one experimental series, IL-2-pre-stimulated NK cells (2×10^5 cells/well) were pulsed with 40 μg/mL GalN or, GalNAc oligomers [48] or chitosan (Sigma-Aldrich St. Louis, MO, USA, #448877) for 24 h at 37˚C and 5% CO_2. For flow cytometric analysis of degranulation, brefeldin A (4 μg/mL, Sigma-Aldrich St. Louis, MO, USA, #B7651), BD GolgiStop (0.67 μL/mL, BD Biosciences, San Jose, CA, USA, Cat#554724), and CD107a-PE (0.5 μL/mL, Miltenyi Biotec, Bergisch Gladbach, Germany, Cat# 130-111-621, RRIDAB_2654474) were added after 6 h of incubation. A combination of 25 ng/mL phorbol-12-myristate-13-acetate (PMA, Sigma-Aldrich St. Louis, MO, USA, # P1585) and 1 μg/mL ionomycin (Sigma-Aldrich St. Louis, MO, USA, # I0634) served as positive control. NK-cell activation was analyzed by flow cytometry and ELISA, as described below.

NK-cell infection assays

IL-2-pre-stimulated NK cells (2×10^5 cells) were incubated with *A*. *fumigatus* (WT, Δ*agd3*, or Δ*uge3*) or *A*. *nidulans* germ tubes at MOIs of 0.5, 2, or 4 for 6 h at 37˚C, unless indicated otherwise. For one experimental series (see Fig 5), *A*. *fumigatus* germ tubes were pre-incubated with either 2 μM Sph3 hydrolase [36], 1 μM Ega3 hydrolase [37], 0.1 μM Agd3 deacetylase [38], or a combination of these enzymes for 30 min, followed by co-culture with NK cells at an MOI of 0.5. All tested co-culture conditions are summarized in S1 Table. For flow cytometric analysis of degranulation, brefeldin A (4 μg/mL), BD GolgiStop (0.67 μL/mL), and CD107a-PE (0.5 μL/mL) were added after 1 h of incubation.

Stimulation of PMN oxidative burst and phagocytosis by NK-cell supernatants

To generate culture supernatants, 2×10^5 NK cells were incubated with 40 μg/mL PGG for 24 h in a 200- μL volume. NK cells were centrifuged at 300 ×*g* for 10 min; supernatant was harvested and stored at– 80˚C until further use. To assess oxidative burst, 2×10^5 isolated PMNs (2×10^6 cells/mL) were incubated with *A*. *fumigatus* ATCC46645 germ tubes (MOI 0.5) in a total of 25 μL RPMI + 10% FCS or seeded in an equivalent volume of RPMI + 10% FCS without fungal cells in a 96-well plate. Next, culture supernatant of NK cell-PGG co-cultures or NK cells cultured alone (40 μL, containing secreted metabolites of 40.000 NK cells) were added. The volume of each well was adjusted to 200 μL with cell-free RPMI + 10% FCS. A combination of 5 ng/mL PMA and 0.2 μg/mL ionomycin served as positive control. ROS production was analyzed by flow cytometry, as described below. To assess phagocytosis, 2×10^5 PMNs were seeded in 96-well plate. Culture supernatant of NK cell-PGG co-cultures or NK cells cultured alone (40 μL, containing secreted metabolites of 40.000 NK cells) and *A*. *fumigatus* (ATCC46645-GFP) conidia were added at an MOI of 3 for 1 h at 37˚C. The volume of each well was adjusted to 200 μL with cell-free RPMI + 10% FCS. Phagocytosis rate was determined using flow cytometry.

RNA isolation and bulk transcriptomic profiling

Total RNA from purified NK cells was isolated using QIAshredder columns (Qiagen, Hilden, Germany, Cat#79656) and the RNeasy Plus Mini Kit (Qiagen, Hilden, Germany, Cat#74136) following the manufacturer's protocol. RNA purity and concentration were tested with a NanoDrop ND-1000 spectral photometer (Thermo Fisher Scientific, Waltham, MA, USA).

The integrity of RNA was determined with a 2100 Bioanalyzer (Agilent Technologies, Waldbronn, Germany) using RNA 6000 Pico or Nano LabChip Kits (Agilent Technologies, Waldbronn, Germany) according to the manufacturer's instructions. RIN values of our samples were in the range of 7.3–10.0, indicating good quality of the RNA samples.

Library preparation was performed with the Illumina TruSeq Stranded mRNA technology, according to the manufacturer's protocol. RNA sequencing was performed by IMGM Laboratories GmbH (Martinsried, Germany) on the Illumina NextSeq 500 next-generation sequencing system with 1×75 bp single-read chemistry. Raw files are accessible under the Gene Expression Omnibus accession number GSE241020.

RNA-seq data processing and analysis

Preprocessing of raw reads, including quality control and gene abundance estimation, was performed with the GEO2RNAseq pipeline (v0.100.1) [59] in R version 3.5.1. Quality analysis was performed before and after trimming with FastQC (v0.11.7). Read-quality trimming was performed with Trimmomatic (v0.36). Adapter sequences were removed, window size trimming was performed (15 nucleotides, average $Q < 25$), 5′ and 3′ clipping was performed for any base with $Q < 3$, and sequences shorter than 30 nucleotides were removed. Reads were mapped against the human reference genome (GRCH 38, v109). First, the reference genome was indexed with exon information using HiSat2 (v2.1.0). Then, read alignment was performed using HiSat2 on the exon-indexed reference genome. Gene abundance estimation was performed with featureCounts (R package Rsubread, v1.34.0) in single-end mode with default parameters. MultiQC (v1.7) was used to summarize the output of FastQC, Trimmomatic, HiSat, featureCounts, and SAMtools. Count matrices were normalized using median-by-ratio normalization (MRN) as described before [60]. Differential gene expression was analyzed by applying DESeq2 (v1.38.3) and adding donor origin as co-factor to the statistical design. Gene expression differences were considered significant at an adjusted p-value of ≤ 0.05. Hierarchical clustering was performed with the ward.D2 clustering method using MRN gene-abundance data with the R package ComplexHeatmap (v2.14.0).

Flow cytometry

NK-cell activation and degranulation as well as neutrophil activation were assessed by flow cytometry. Therefore, NK-cell/PMN cultures were centrifuged for 10 min at 300 ×*g* at RT and cell pellets were resuspended in 100 μL HBSS supplemented with 2 mM EDTA and 1% FCS. Cells were stained extracellularly with fluorescent antibodies listed in S2 Table and the fixable Viobility Live/Dead Dye (Miltenyi Biotec, Bergisch Gladbach, Germany, Cat#130-110-205). After incubation in the dark for 15 min at 4˚C, cells were washed with 2 mL HBSS supplemented with 2 mM EDTA and 1% FCS, resuspended in 150 μL of 4% paraformaldehyde (Sigma-Aldrich, St. Louis, MO, USA, #47608), and incubated for 30 min at RT. Intracellular staining was performed using the Inside Stain Kit (Miltenyi Biotec, Bergisch Gladbach, Germany, Cat#130-090-477). After extracellular staining, cells were washed with 2 mL HBSS supplemented with 2 mM EDTA and 1% FCS, resuspended in 300 μL of Inside Fix solution (150 μL Inside Fix and 150μL HBSS + EDTA), and incubated for 20 min at RT. After washing, 100 μL of intracellular staining mix in Inside Perm was added and cells were incubated for 10 min at RT in the dark. Cells were washed with 750 μL Inside Perm and resuspended in 150 μL of HBSS with EDTA. Data were acquired on a FACSCalibur (Treestar/Becton & Dickinson, BD), Cytoflex flow cytometer (Beckman Coulter, Brea, CA, USA) or MACS Quant 10 flow cytometer (Miltenyi Biotec, Bergisch Gladbach, Germany). Downstream data analysis was performed with FlowJo10 (Treestar/Becton & Dickinson, BD) or Kaluza v.2.1 (Beckman Coulter,

Brea, CA, USA). Gating strategies and representative raw data are shown in S2, S3, S4 and S5 Figs.

ELISA and multiplex cytokine assay

To quantify cytokine and chemokine release of stimulated NK cells, cell cultures were harvested and centrifuged at 300 ×*g* for 10 min. Culture supernatants were cryopreserved at -80˚C until further analysis. Concentrations of CCL3 (MIP-1α, R&D Systems, Minneapolis, MN, USA, #DY270-05), CCL4 (MIP-1β, R&D Systems, Minneapolis, MN, USA, #DY271-05), CCL5 (RANTES, Biolegend, San Diego, CA, USA, Cat#440804), IFN-ɣ (Biolegend, San Diego, CA, USA, Cat#430104), granzyme B (R&D Systems, Minneapolis, MN, USA, #DY2906-05), and perforin (abcam, Cambridge, UK, #ab83709) were determined using ELISA kits according to the manufacturer's manual with minor modifications. Briefly, ELISAs were performed in 96-well half-area, high-binding plates with one-fourth of the volume recommended by the manufacturer. Absorbance was measured with a NanoQuant Infinite 200M Pro microplate reader (Tecan, Maennedorf, Switzerland). For multiplexed quantification of cytokine and chemokine concentrations in supernatants of NK cells infected with enzymatically pre-treated *A. fumigatus*, a ProcartaPlex 11-PLEX assay kit (ThermoFisher Scientific, Waltham, MA, USA, Cat#PPX-11) including GM-CSF, granzyme B, IFN-ɣ, IL-1α, IL-6, IL-8, CCL3, CCL4, perforin, CCL5, TNF-α was used according to the manufacturer's instructions. Acquisition/measurement was performed using a Luminex detection system (Bio-Plex 200 system) and Bio-Plex Manager Software 6.2 (Bio-Rad, Hercules, CA, USA).

Binding of soluble CD56 to *A. fumigatus* hyphae

Cellvis 8-well (Mountain View, CA, USA) coverslips were pre-coated with laminin (20 μg/mL, Sigma Aldrich, St. Louis, MO, USA, #L2020) for 1 h at 33˚C and washed twice with ddH_2O. *A. fumigatus* Af293, *Δagd3*, and *Δuge3* conidia were suspended in colorless RPMI (Gibco, Thermo Fisher Scientific, Waltham, MA, USA, #11835030), added to the coated coverslips (5×10^4 per well), and incubated at 33˚C until germination. Hyphae were incubated with soluble CD56 (5 μg/mL, R&D Systems, Minneapolis, MN, USA, Cat#2408-NC) or BSA (control, 5 μg/mL, Roth, Karlsruhe, Germany, #0163.2) in colorless RPMI for 2 h at 37˚C, 5% CO_2. Wells were washed twice with colorless RPMI, fixed with 1% formaldehyde (Thermo Fisher Scientific, Waltham, MA, USA, #28906) for 10 min, and washed once with HBSS. After blocking with 5% BSA in HBSS for 30 min, samples were stained with Alexa Fluor 647-labeled mouse-anti-human CD56 (10 μg/mL, Biolegend, San Diego, CA, USA, #318314) for 1 h and washed with HBSS. Stained samples were imaged with an LSM700 laser scanning confocal microscope (Carl Zeiss, Jena, Germany) with a plan-apochromat 63x/1.40 oil immersion objective. The following acquisition settings were used: image size, 71.35×71.35 μm; laser power, 8%; gain, 650; pinhole, 1 AU (53.7). Z-stacks were obtained at an interval of 1–2 μm. ImageJ/Fiji software was used for image processing.

Fluorescence microscopy of NK-cell/*A. fumigatus* co-cultures

A. fumigatus Af293 and *Δagd3*, (5×10^4 conidia per well in colorless RPMI) were seeded on laminin-coated (20 μg/mL) 8-well coverslips and incubated overnight at 33˚C to enable germination, as described above. NK cells were added to the germ tubes at an MOI of 0.5 (1×10^5 cells per well) and incubated for 4 h at 37˚C, 5% CO_2. After incubation, samples were fixed with 1% formaldehyde for 7 min, washed once with PBS, and blocked with 2.5% BSA in PBS for 30 min. Samples were stained immediately after fixation with Alexa Fluor 647-labeled mouse-anti-human CD56 (10 μg/mL) for 1 h and washed with PBS. CLSM images were

recorded with a LSM700 system (Carl Zeiss, Jena, Germany) using a plan-apochromat 63 ×/1.40 oil immersion objective.

IncuCyte imaging

To generate culture supernatants for IncuCyte experiments, 2×10^5 NK cells were incubated with 40 μg/mL PGG for 24 h in a 200-μL volume. NK cells were centrifuged at 300 ×*g* for 10 min; supernatant was harvested and stored at– 80˚C until further use. For IncuCyte experiments, *A*. *fumigatus* spores (ATCC46645-GFP) were diluted in RPMI + 10% FCS to a final concentration of 3×10^3/mL. Fifty microliters (150 conidia/well) were dispensed per well of a 96-well flat-bottom plate. To test the direct antifungal effect of PGG-pulsed NK cells, culture supernatant of NK cell-PGG co-cultures or NK cells cultured alone (37.5 μL, containing secreted metabolites of 37,500 NK cells) was added to the wells. The volume of each well was adjusted to 150 μL with cell-free RPMI + 10% FCS. To evaluate the capacity of PGG-stimulated NK cells to enhance fungal growth inhibition by PMNs, 1.5×10^4 PMNs (effector/target ratio, 100) in 85 μL RPMI + 10% FCS were added to the wells. In addition, culture supernatant of NK cell-PGG co-cultures or NK cell cultured alone (15 μL, containing secreted metabolites of 15,000 NK cells) was added to the wells. The volume of each well was adjusted to 150 μL with cell-free RPMI + 10% FCS. In addition to biological replicates (n = 5), each condition was tested in technical duplicates. IncuCyte microscopy and NeuroTrack-based image analysis (IncuCyte Zoom NeuroTrack software module) was performed according to Wurster *et al*. [39]. In brief, well plates were imaged hourly in the IncuCyte Zoom HD/2CLR time-lapse microscopy system (Sartorius, Göttingen, Germany) equipped with an IncuCyte Zoom 10× Plan Fluor objective (Sartorius, Göttingen, Germany) for a period of 16 h. Acquisition time for the green channel was 400 ms. The following parameters were used for NeuroTrack analysis: neurite coarse sensitivity, 5; neurite fine sensitivity, 0.25; neurite width, 4 μm. Neurite length [mm/mm^2] and numbers of branch points [$1/mm^2$]) were compared to an "*A*. *fumigatus* only" control without NK-cell supernatants and/or PMNs.

Statistical analyses

Microsoft Excel 365, GraphPad Prism version 9, and R version 3.5.1 were used for data compilation, analysis, and visualization. Significance testing was performed using one-way analysis of variance (ANOVA), repeated measures one-way ANOVA, and paired t-test for unmatched multi-group comparisons, matched multi-group comparisons, and matched two-group comparisons, respectively. For multi-group comparisons, Dunnett's or Tukey's post-hoc tests were used for experiments with a single control group or analysis of all pairwise comparisons, respectively. Significance tests are specified in the figure legends. (Adjusted) p-values < 0.05 were considered significant.

Supporting information

S1 Fig. Interaction of CD56 with galactosaminogalactan to trigger NK-cell activation. (A) Concentration dependent interaction of CD56 with galactosaminogalactan (GAG) N = 3 technical replicates, with two batches of GAG. (**B**) CD56 binding to GAG, with and without pre-incubation with GAG oligosaccharide fractions. N = 2 technical replicates. (**C**) Intracellular IFN-γ levels of naïve NK cells (Control) and NK cells stimulated for 24 h with different concentrations of urea-insoluble galactosaminogalactan (PGG). Representative histograms and data for 4 independent donors are shown. Release of IFN-γ (**D**), granzyme B (**E**) and perforin (**F**) by naïve NK cells (Control) and NK cells stimulated for 24 h with different concentrations of PGG. N = 3 independent donors. Columns and error bars indicate means and standard

deviations, respectively. Repeated measures one-way ANOVA with Tukey's post-hoc test. * $p < 0.05$, ** $p < 0.01$, *** $p < 0.001$.
(TIF)

S2 Fig. Applied gating strategy for flow cytometric analysis to study NK cell interaction, activation, and degranulation. Isolated Lymphocytes are selected according to their forward and side scattering and single lymphocytes were gated based on SSC-A, and SSC-H properties. Dead lymphocytes were excluded by Live/Dead staining. Natural killer (NK) cells were identified as $CD3^-$. Positive cells for NK cell surface marker CD56, for activation markers CD69, and degranulation marker CD107a were gated within each $CD3^-$ NK cell population. Fluorescence positivity was determined for all markers.
(TIF)

S3 Fig. Applied gating strategy for flow cytometric analysis to investigate NK cell interaction and intracellular IFN-γ production. Lymphocytes are selected according to their forward and side scattering and single lymphocytes were gated based on SSC-A, and SSC-H properties. Dead lymphocytes were removed from the living cell population by Live/Dead staining. Natural killer (NK) cells were determined as $CD3^-$. $CD3^-$ are further characterized regarding expression of the NK cell surface marker CD56, and intracellular IFN-γ levels. Fluorescence positivity was determined for all markers.
(TIF)

S4 Fig. Applied gating strategy to determine ROS production by PMNs. Debris was excluded from isolated granulocytes by light scatter properties and dead granulocytes were excluded by Live/Dead staining. Granulocytes were identified by CD66 expression and analyzed for ROS expression. Fluorescence positivity was determined for ROS.
(TIF)

S5 Fig. Applied gating strategy to for flow cytometric analysis to study phagocytosis. Isolated granulocytes are selected according to their forward and side scattering and single lymphocytes were gated based on SSC-A, and SSC-H properties. Conidia phagocytosed by PMNs are identified as $CD66b^+GFP^+$.
(TIF)

S1 Table. Preparation of NK cell *A. fumigatus*-infection assay with wild type Af293 or Δ*agd3*/ Δ*uge3* mutants and their enzymatic pre-treatment. X indicates that the compound was used for the respective condition. A total volume of 200 μL was used for all conditions. Abbreviations: gt = germ tubes, PMA = Phorbol-12-myristate-13-acetate, RPMI = Roswell Park Memorial Institute medium, n/a = not applicable.
(DOCX)

S2 Table. Detailed information about antibodies used for flow cytometric analyses All antibodies/dyes were used at 1% v/v, except for CD69 PercP (2% v/v), and CD3 PE (2% v/v).
(DOCX)

S1 Data. Detailed information about generated raw dataset of Fig 1.
(XLSX)

S2 Data. Detailed information about generated raw dataset of Fig 2.
(XLSX)

S3 Data. Detailed information about the generated primary material of Fig 3.
(XLSX)

S4 Data. Detailed information about generated raw dataset shown in Fig 4.
(XLSX)

S5 Data. Detailed information about raw dataset used to generate Fig 5.
(XLSX)

S6 Data. Detailed information about the generated primary material of Fig 6.
(XLSX)

S7 Data. Detailed information about raw dataset used to generate S1 Fig.
(XLSX)

Acknowledgments

The authors wish to thank all blood donors.

We thank Jean-Paul Latgé, Institute of Molecular Biology and Biotechnology (IMBBFORTH), University of Crete, Heraklion, Greece, for his great support and advice in the preparation of this manuscript.

Author Contributions

Conceptualization: Linda Heilig, Vishukumar Aimanianda, Thierry Fontaine, Ulrich Terpitz, François Le Mauff, Donald C. Sheppard, Oliver Kurzai, Sebastian Wurster, Juergen Loeffler.

Data curation: Linda Heilig, Sascha Schäuble, Sebastian Wurster.

Formal analysis: Linda Heilig, Fariha Natasha, Nora Trinks, Vishukumar Aimanianda, Sarah Sze Wah Wong, Sascha Schäuble, Esther Weiss, Sebastian Wurster.

Funding acquisition: Ulrich Terpitz, Hermann Einsele, Juergen Loeffler.

Investigation: Linda Heilig, Fariha Natasha, Nora Trinks, Vishukumar Aimanianda, Sarah Sze Wah Wong, Lea Strobel, Sascha Schäuble, Kerstin Hünniger, Esther Weiss.

Methodology: Linda Heilig, Fariha Natasha, Nora Trinks, Vishukumar Aimanianda, Sarah Sze Wah Wong, Lea Strobel, Sascha Schäuble, Kerstin Hünniger, Esther Weiss, Mario Vargas.

Project administration: Thierry Fontaine, Sebastian Wurster, Juergen Loeffler.

Resources: Vishukumar Aimanianda, Thierry Fontaine, François Le Mauff, Donald C. Sheppard, Mario Vargas, P. Lynne Howell, Juergen Loeffler.

Software: Linda Heilig, Sascha Schäuble, Sebastian Wurster.

Supervision: Vishukumar Aimanianda, Thierry Fontaine, Ulrich Terpitz, François Le Mauff, Donald C. Sheppard, Oliver Kurzai, P. Lynne Howell, Gianni Panagiotou, Sebastian Wurster, Hermann Einsele.

Validation: Linda Heilig, Vishukumar Aimanianda, Sascha Schäuble, Sebastian Wurster.

Visualization: Linda Heilig, Fariha Natasha, Nora Trinks, Vishukumar Aimanianda, Ulrich Terpitz, Sascha Schäuble, Sebastian Wurster.

Writing – original draft: Linda Heilig, Sebastian Wurster, Juergen Loeffler.

Writing – review & editing: Linda Heilig, Vishukumar Aimanianda, Thierry Fontaine, Ulrich Terpitz, François Le Mauff, Donald C. Sheppard, Sascha Schäuble, Oliver Kurzai, Kerstin Hünniger, Sebastian Wurster, Hermann Einsele, Juergen Loeffler.

References

1. Corre E, Carmagnat M, Busson M, de Latour RP, Robin M, Ribaud P, et al. Long-term immune deficiency after allogeneic stem cell transplantation: B-cell deficiency is associated with late infections. Haematologica. 2010; 95(6):1025–9. Epub 2010/02/06. https://doi.org/10.3324/haematol.2009.018853 PMID: 20133894; PubMed Central PMCID: PMC2878804.
2. Singh N, Paterson DL. Aspergillus infections in transplant recipients. Clinical microbiology reviews. 2005; 18(1):44–69. Epub 2005/01/18. https://doi.org/10.1128/CMR.18.1.44-69.2005 PMID: 15653818; PubMed Central PMCID: PMC544171.
3. Segal BH. Aspergillosis. 2009; 360(18):1870–84. https://doi.org/10.1056/NEJMra0808853 PMID: 19403905.
4. Cunha C, Carvalho A. Genetic defects in fungal recognition and susceptibility to invasive pulmonary aspergillosis. Medical mycology. 2019; 57(Supplement_2):S211–s8. Epub 2019/03/01. https://doi.org/10.1093/mmy/myy057 PMID: 30816966.
5. Helleberg M, Steensen M, Arendrup MC. Invasive aspergillosis in patients with severe COVID-19 pneumonia. Clinical microbiology and infection: the official publication of the European Society of Clinical Microbiology and Infectious Diseases. 2021; 27(1):147–8. Epub 2020/08/10. https://doi.org/10.1016/j.cmi.2020.07.047 PMID: 32768493; PubMed Central PMCID: PMC7403849.
6. Osherov N, Kontoyiannis DP. The anti-Aspergillus drug pipeline: Is the glass half full or empty? Medical mycology. 2017; 55(1):118–24. Epub 2016/08/27. https://doi.org/10.1093/mmy/myw060 PMID: 27562862.
7. Boyer J, Feys S, Zsifkovits I, Hoenigl M, Egger M. Treatment of Invasive Aspergillosis: How It's Going, Where It's Heading. Mycopathologia. 2023. https://doi.org/10.1007/s11046-023-00727-z PMID: 37100963
8. Sun KS, Tsai CF, Chen SC, Huang WC. Clinical outcome and prognostic factors associated with invasive pulmonary aspergillosis: An 11-year follow-up report from Taiwan. PloS one. 2017; 12(10): e0186422. Epub 2017/10/20. https://doi.org/10.1371/journal.pone.0186422 PMID: 29049319; PubMed Central PMCID: PMC5648178.
9. Salmeron G, Porcher R, Bergeron A, Robin M, Peffault de Latour R, Ferry C, et al. Persistent poor long-term prognosis of allogeneic hematopoietic stem cell transplant recipients surviving invasive aspergillosis. Haematologica. 2012; 97(9):1357–63. Epub 2012/03/01. https://doi.org/10.3324/haematol.2011.058255 PMID: 22371177; PubMed Central PMCID: PMC3436236.
10. Lehrnbecher T, Schmidt S. Why are natural killer cells important for defense against Aspergillus? Medical mycology. 2019; 57(Supplement_2):S206–S10. https://doi.org/10.1093/mmy/myy034 PMID: 30816962
11. Schmidt S, Zimmermann SY, Tramsen L, Koehl U, Lehrnbecher T. Natural killer cells and antifungal host response. Clinical and vaccine immunology: CVI. 2013; 20(4):452–8. Epub 2013/02/01. https://doi.org/10.1128/cvi.00606-12 PMID: 23365210; PubMed Central PMCID: PMC3623417.
12. Stuehler C, Kuenzli E, Jaeger VK, Baettig V, Ferracin F, Rajacic Z, et al. Immune Reconstitution After Allogeneic Hematopoietic Stem Cell Transplantation and Association With Occurrence and Outcome of Invasive Aspergillosis. The Journal of Infectious Diseases. 2015; 212(6):959–67. https://doi.org/10.1093/infdis/jiv143 J The Journal of Infectious Diseases. PMID: 25748323
13. Caligiuri MA. Human natural killer cells. Blood. 2008; 112(3):461–9. Epub 2008/07/25. https://doi.org/10.1182/blood-2007-09-077438 PMID: 18650461; PubMed Central PMCID: PMC2481557.
14. Vivier E, Tomasello E, Baratin M, Walzer T, Ugolini S. Functions of natural killer cells. Nature immunology. 2008; 9(5):503–10. Epub 2008/04/22. https://doi.org/10.1038/ni1582 PMID: 18425107.
15. Krzewski K, Strominger JLJCoicb. The killer's kiss: the many functions of NK cell immunological synapses. 2008; 20 5:597–605.
16. Khosravi-Far R, Esposti MD. Death receptor signals to mitochondria. Cancer biology & therapy. 2004; 3 (11):1051–7. Epub 2005/01/11. https://doi.org/10.4161/cbt.3.11.1173 PMID: 15640619; PubMed Central PMCID: PMC2941887.
17. Voigt J, Hünniger K, Bouzani M, Jacobsen ID, Barz D, Hube B, et al. Human Natural Killer Cells Acting as Phagocytes Against Candida albicans and Mounting an Inflammatory Response That Modulates Neutrophil Antifungal Activity. The Journal of Infectious Diseases. 2013; 209(4):616–26. https://doi.org/10.1093/infdis/jit574 J The Journal of Infectious Diseases. PMID: 24163416

18. Schmidt S, Tramsen L, Lehrnbecher T. Natural Killer Cells in Antifungal Immunity. 2017; 8. https://doi.org/10.3389/fimmu.2017.01623 PMID: 29213274

19. Ma LL, Wang CLC, Neely GG, Epelman S, Krensky AM, Mody CH. NK Cells Use Perforin Rather than Granulysin for Anticryptococcal Activity1. The Journal of Immunology. 2004; 173(5):3357–65. https://doi.org/10.4049/jimmunol.173.5.3357% J The Journal of Immunology. PMID: 15322199

20. Trinks N, Reinhard S, Drobny M, Heilig L, Löffler J, Sauer M, et al. Subdiffraction-resolution fluorescence imaging of immunological synapse formation between NK cells and A. fumigatus by expansion microscopy. Commun Biol. 2021; 4(1):1151. Epub 2021/10/06. https://doi.org/10.1038/s42003-021-02669-y PMID: 34608260; PubMed Central PMCID: PMC8490467.

21. Campbell KS, Hasegawa J. Natural killer cell biology: An update and future directions. Journal of Allergy and Clinical Immunology. 2013; 132(3):536–44. https://doi.org/10.1016/j.jaci.2013.07.006 PMID: 23906377

22. Paul S, Lal G. The Molecular Mechanism of Natural Killer Cells Function and Its Importance in Cancer Immunotherapy. 2017; 8. https://doi.org/10.3389/fimmu.2017.01124 PMID: 28955340

23. Li SS, Ogbomo H, Mansour MK, Xiang RF, Szabo L, Munro F, et al. Identification of the fungal ligand triggering cytotoxic PRR-mediated NK cell killing of Cryptococcus and Candida. Nature Communications. 2018; 9(1):751. https://doi.org/10.1038/s41467-018-03014-4 PMID: 29467448

24. Vitenshtein A, Charpak-Amikam Y, Yamin R, Bauman Y, Isaacson B, Stein N, et al. NK Cell Recognition of Candida glabrata through Binding of NKp46 and NCR1 to Fungal Ligands Epa1, Epa6, and Epa7. Cell Host & Microbe. 2016; 20(4):527–34. https://doi.org/10.1016/j.chom.2016.09.008 PMID: 27736647

25. Ziegler S, Weiss E, Schmitt AL, Schlegel J, Burgert A, Terpitz U, et al. CD56 Is a Pathogen Recognition Receptor on Human Natural Killer Cells. Scientific reports. 2017; 7(1):6138. Epub 2017/07/25. https://doi.org/10.1038/s41598-017-06238-4 PMID: 28733594; PubMed Central PMCID: PMC5522490.

26. Janeway CA Jr. Approaching the asymptote? Evolution and revolution in immunology. Cold Spring Harbor symposia on quantitative biology. 1989; 54 Pt 1:1–13. Epub 1989/01/01. https://doi.org/10.1101/sqb.1989.054.01.003 PMID: 2700931.

27. van de Veerdonk FL, Gresnigt MS, Romani L, Netea MG, Latge JP. Aspergillus fumigatus morphology and dynamic host interactions. Nat Rev Microbiol. 2017; 15(11):661–74. Epub 2017/09/19. https://doi.org/10.1038/nrmicro.2017.90 PMID: 28919635.

28. Latgé J-P, Chamilos G. Aspergillus fumigatus and Aspergillosis in 2019. 2019; 33(1):10.1128/cmr.00140-18. https://doi.org/10.1128/CMR.00140-18 PMID: 31722890

29. Fontaine T, Delangle A, Simenel C, Coddeville B, van Vliet SJ, van Kooyk Y, et al. Galactosaminogalactan, a New Immunosuppressive Polysaccharide of Aspergillus fumigatus. PLOS Pathogens. 2011; 7(11):e1002372. https://doi.org/10.1371/journal.ppat.1002372 PMID: 22102815

30. Speth C, Rambach G, Lass-Flörl C, Howell PL, Sheppard DC. Galactosaminogalactan (GAG) and its multiple roles in Aspergillus pathogenesis. Virulence. 2019; 10(1):976–83. https://doi.org/10.1080/21505594.2019.1568174 PMID: 30667338

31. Lee MJ, Liu H, Barker BM, Snarr BD, Gravelat FN, Al Abdallah Q, et al. The Fungal Exopolysaccharide Galactosaminogalactan Mediates Virulence by Enhancing Resistance to Neutrophil Extracellular Traps. PLOS Pathogens. 2015; 11(10):e1005187. https://doi.org/10.1371/journal.ppat.1005187 PMID: 26492565

32. Lee MJ, Geller AM, Bamford NC, Liu H, Gravelat FN, Snarr BD, et al. Deacetylation of Fungal Exopolysaccharide Mediates Adhesion and Biofilm Formation. 2016; 7(2):e00252–16. https://doi.org/10.1128/mBio.00252-16 PMID: 27048799

33. Gravelat FN, Beauvais A, Liu H, Lee MJ, Snarr BD, Chen D, et al. Aspergillus Galactosaminogalactan Mediates Adherence to Host Constituents and Conceals Hyphal β-Glucan from the Immune System. PLOS Pathogens. 2013; 9(8):e1003575. https://doi.org/10.1371/journal.ppat.1003575 PMID: 23990787

34. Vunain E, Mishra AK, Mamba BB. 1—Fundamentals of chitosan for biomedical applications. In: Jennings JA, Bumgardner JD, editors. Chitosan Based Biomaterials Volume 1: Woodhead Publishing; 2017. p. 3–30.

35. Hoemann CD, Fong D. 3—Immunological responses to chitosan for biomedical applications. In: Jennings JA, Bumgardner JD, editors. Chitosan Based Biomaterials Volume 1: Woodhead Publishing; 2017. p. 45–79.

36. Bamford NC, Snarr BD, Gravelat FN, Little DJ, Lee MJ, Zacharias CA, et al. Sph3 Is a Glycoside Hydrolase Required for the Biosynthesis of Galactosaminogalactan in Aspergillus fumigatus. The Journal of biological chemistry. 2015; 290(46):27438–50. Epub 2015/09/06. https://doi.org/10.1074/jbc.M115.679050 PMID: 26342082; PubMed Central PMCID: PMC4645995.

37. Bamford NC, Le Mauff F, Subramanian AS, Yip P, Millán C, Zhang Y, et al. Ega3 from the fungal pathogen Aspergillus fumigatus is an endo-α-1,4-galactosaminidase that disrupts microbial biofilms. The Journal of biological chemistry. 2019; 294(37):13833–49. Epub 2019/08/17. https://doi.org/10.1074/jbc.RA119.009910 PMID: 31416836; PubMed Central PMCID: PMC6746457.

38. Bamford NC, Le Mauff F, Van Loon JC, Ostapska H, Snarr BD, Zhang Y, et al. Structural and biochemical characterization of the exopolysaccharide deacetylase Agd3 required for Aspergillus fumigatus biofilm formation. Nature Communications. 2020; 11(1):2450. https://doi.org/10.1038/s41467-020-16144-5 PMID: 32415073

39. Wurster S, Kumaresan PR, Albert ND, Hauser PJ, Lewis RE, Kontoyiannis DP. Live Monitoring and Analysis of Fungal Growth, Viability, and Mycelial Morphology Using the IncuCyte NeuroTrack Processing Module. mBio. 2019; 10(3). Epub 2019/05/30. https://doi.org/10.1128/mBio.00673-19 PMID: 31138745; PubMed Central PMCID: PMC6538782.

40. Taouk G, Hussein O, Zekak M, Abouelghar A, Al-Sarraj Y, Abdelalim EM, et al. CD56 expression in breast cancer induces sensitivity to natural killer-mediated cytotoxicity by enhancing the formation of cytotoxic immunological synapse. Scientific reports. 2019; 9(1):8756. https://doi.org/10.1038/s41598-019-45377-8 PMID: 31217484

41. Valgardsdottir R, Capitanio C, Texido G, Pende D, Cantoni C, Pesenti E, et al. Direct involvement of CD56 in cytokine-induced killer–mediated lysis of CD56+ hematopoietic target cells. Experimental Hematology. 2014; 42(12):1013–21.e1. https://doi.org/10.1016/j.exphem.2014.08.005 PMID: 25201755

42. Reiners KS, Topolar D, Henke A, Simhadri VR, Kessler J, Sauer M, et al. Soluble ligands for NK cell receptors promote evasion of chronic lymphocytic leukemia cells from NK cell anti-tumor activity. Blood. 2013; 121(18):3658–65. Epub 2013/03/20. https://doi.org/10.1182/blood-2013-01-476606 PMID: 23509156; PubMed Central PMCID: PMC3643764.

43. Gunesch JT, Dixon AL, Ebrahim TA, Berrien-Elliott MM, Tatineni S, Kumar T, et al. CD56 regulates human NK cell cytotoxicity through Pyk2. eLife. 2020; 9. Epub 2020/06/09. https://doi.org/10.7554/eLife.57346 PMID: 32510326; PubMed Central PMCID: PMC7358009.

44. Schmidt S, Tramsen L, Hanisch M, Latgé J-P, Huenecke S, Koehl U, et al. Human Natural Killer Cells Exhibit Direct Activity Against Aspergillus fumigatus Hyphae, But Not Against Resting Conidia. The Journal of Infectious Diseases. 2011; 203(3):430–5. https://doi.org/10.1093/infdis/jiq062 J The Journal of Infectious Diseases. PMID: 21208932

45. Sheppard DC. Molecular mechanism of Aspergillus fumigatus adherence to host constituents. Current Opinion in Microbiology. 2011; 14(4):375–9. https://doi.org/10.1016/j.mib.2011.07.006 PMID: 21784698

46. Christin L, Wysong DR, Meshulam T, Hastey R, Simons ER, Diamond RD. Human platelets damage Aspergillus fumigatus hyphae and may supplement killing by neutrophils. Infection and immunity. 1998; 66(3):1181–9. Epub 1998/03/06. https://doi.org/10.1128/IAI.66.3.1181-1189.1998 PMID: 9488412; PubMed Central PMCID: PMC108032.

47. Rambach G, Blum G, Latgé JP, Fontaine T, Heinekamp T, Hagleitner M, et al. Identification of Aspergillus fumigatus Surface Components That Mediate Interaction of Conidia and Hyphae With Human Platelets. J Infect Dis. 2015; 212(7):1140–9. Epub 2015/03/27. https://doi.org/10.1093/infdis/jiv191 PMID: 25810442.

48. Gressler M, Heddergott C, N'Go IC, Renga G, Oikonomou V, Moretti S, et al. Definition of the Anti-inflammatory Oligosaccharides Derived From the Galactosaminogalactan (GAG) From Aspergillus fumigatus. Frontiers in cellular and infection microbiology. 2019; 9:365. Epub 2019/11/30. https://doi.org/10.3389/fcimb.2019.00365 PMID: 31781511; PubMed Central PMCID: PMC6851199.

49. Briard B, Fontaine T, Samir P, Place DE, Muszkieta L, Malireddi RKS, et al. Galactosaminogalactan activates the inflammasome to provide host protection. Nature. 2020; 588(7839):688–92. Epub 2020/12/04. https://doi.org/10.1038/s41586-020-2996-z PMID: 33268895; PubMed Central PMCID: PMC8086055.

50. Picard LK, Claus M, Fasbender F, Watzl C. Human NK cells responses are enhanced by CD56 engagement. European journal of immunology. 2022; 52(9):1441–51. Epub 2022/07/02. https://doi.org/10.1002/eji.202249868 PMID: 35775327.

51. Robinet P, Baychelier F, Fontaine T, Picard C, Debré P, Vieillard V, et al. A polysaccharide virulence factor of a human fungal pathogen induces neutrophil apoptosis via NK cells. Journal of immunology (Baltimore, Md: 1950). 2014; 192(11):5332–42. Epub 2014/05/03. https://doi.org/10.4049/jimmunol.1303180 PMID: 24790151.

52. Gresnigt MS, Bozza S, Becker KL, Joosten LA, Abdollahi-Roodsaz S, van der Berg WB, et al. A polysaccharide virulence factor from Aspergillus fumigatus elicits anti-inflammatory effects through induction of Interleukin-1 receptor antagonist. PLoS Pathog. 2014; 10(3):e1003936. Epub 2014/03/08.

https://doi.org/10.1371/journal.ppat.1003936 PMID: 24603878; PubMed Central PMCID: PMC3946377.

53. Van Acker HH, Capsomidis A, Smits EL, Van Tendeloo VF. CD56 in the Immune System: More Than a Marker for Cytotoxicity? Front Immunol. 2017; 8:892. Epub 2017/08/10. https://doi.org/10.3389/fimmu.2017.00892 PMID: 28791027; PubMed Central PMCID: PMC5522883.

54. Le Mauff F, Bamford NC, Alnabelseya N, Zhang Y, Baker P, Robinson H, et al. Molecular mechanism of Aspergillus fumigatus biofilm disruption by fungal and bacterial glycoside hydrolases. Journal of Biological Chemistry. 2019; 294(28):10760–72. https://doi.org/10.1074/jbc.RA119.008511 PMID: 31167793

55. Costachel C, Coddeville B, Latgé JP, Fontaine T. Glycosylphosphatidylinositol-anchored fungal polysaccharide in Aspergillus fumigatus. The Journal of biological chemistry. 2005; 280(48):39835–42. Epub 2005/10/06. https://doi.org/10.1074/jbc.M510163200 PMID: 16204227.

56. Stephen-Victor E, Karnam A, Fontaine T, Beauvais A, Das M, Hegde P, et al. Aspergillus fumigatus Cell Wall α-(1,3)-Glucan Stimulates Regulatory T-Cell Polarization by Inducing PD-L1 Expression on Human Dendritic Cells. J Infect Dis. 2017; 216(10):1281–94. Epub 2017/10/03. https://doi.org/10.1093/infdis/jix469 PMID: 28968869.

57. Bozza S, Clavaud C, Giovannini G, Fontaine T, Beauvais A, Sarfati J, et al. Immune sensing of Aspergillus fumigatus proteins, glycolipids, and polysaccharides and the impact on Th immunity and vaccination. Journal of immunology (Baltimore, Md: 1950). 2009; 183(4):2407–14. Epub 2009/07/25. https://doi.org/10.4049/jimmunol.0900961 PMID: 19625642.

58. Muszkieta L, Aimanianda V, Mellado E, Gribaldo S, Alcàzar-Fuoli L, Szewczyk E, et al. Deciphering the role of the chitin synthase families 1 and 2 in the in vivo and in vitro growth of Aspergillus fumigatus by multiple gene targeting deletion. Cellular microbiology. 2014; 16(12):1784–805. Epub 2014/06/21. https://doi.org/10.1111/cmi.12326 PMID: 24946720.

59. Seelbinder B, Wolf T, Priebe S, McNamara S, Gerber S, Guthke R, et al. GEO2RNAseq: An easy-to-use R pipeline for complete pre-processing of RNA-seq data. 2019:771063. https://doi.org/10.1101/771063% J bioRxiv.

60. Anders S, Huber W. Differential expression analysis for sequence count data. Genome Biology. 2010; 11(10):R106. https://doi.org/10.1186/gb-2010-11-10-r106 PMID: 20979621